Catena 205 (2021) 105445

Contents lists available at ScienceDirect

Catena

journal homepage: www.elsevier.com/locate/catena

High-resolution analysis of the Likhvin loess-paleosol sequence (the central part of the East European Plain, Russia)

P.G. Panin [a,*], K.G. Filippova [a], A.V. Bukhonov [b], N.V. Karpukhina [a], P.I. Kalinin [b], M. V. Ruchkin [c,d]

[a] Institute of Geography, Russian Academy of Sciences, Staromonetny 29, 119017 Moscow, Russia
[b] Institute of Physicochemical and Biological Problems in Soil Science, Russian Academy of Sciences, Institutskaya 2, 142290 Pushchino, Russia
[c] A.P. Karpinsky Russian Geological Research Institute (FGBU «VSEGEI»), Sredny prospect 74, 199106 St. Petersburg, Russia
[d] Institute of Earth Science, St. Petersburg University, Universitetskaya nab. 7-9, 199034 St. Petersburg, Russia

ARTICLE INFO

Keywords:
Pleistocene
Soil
Changing of the climate
Interglacial
Interstadial
Micromorphology

ABSTRACT

Studies of the loess-paleosol sequence of the center of the East European Plain have a long history. Previously, samples from loess-soil sections were taken for paleoreconstruction of climate and environment with low resolution, usually 1–2 samples per stratigraphic unit. This led to an unclear interpretation of the processes of soil formation and deposition of loess material. Our article discusses the LPS of the Likhvin stratotype section. High-resolution analysis was applied, which will allow us to trace in detail the history of the formation of the paleosol cover from the Middle Pleistocene to the present. A total of 245 bulk samples were taken from sections Likhvin-1/18 and Likhvin-2/18 and analyzed using laboratory analytics (the particle-size distribution, magnetic susceptibility, the loss on ignition values, total organic carbon, pH). Nine samples were taken for OSL dating and two samples for AMS dating to determine the age of the deposits. The micromorphological characteristics were described in detail for paleosols. The Salyn interglacial paleosol (MIS 5e) appeared to be comparable to the modern Retisols in its macro- and micromorphology and physical and chemical characteristics. As to the Krutitsa interstadial paleosol (identified formerly with MIS 5c in the sequence), our results suggest its belonging to MIS 5a. The modern prairie soils – Folic Cambisols – may be considered as its modern analogue. During the MIS 3, the Bryansk paleosol developed. The paleosol is polygenetic; in cooling, its main type (Cambisol) changed to Gleysol and finally became Cryosol. The paleosol described as belonging to MIS 7 displays all the characteristics of the Early Kamenka interglacial paleosol and develops the characteristics of Luvisols (Cutanic) type, its analogues being found in Latvia, Poland, and Hungary. There is a level of soil-formation above the Early Kamenka interglacial paleosol corresponding to the Romny paleosol (MIS 6) in its stratigraphic position. The latter statement is difficult to assert with confidence; it is not improbable that the level presents the Late Kamenka interstadial paleosol, also attributable to MIS 6.

In memoriam of D.Sc. T.D. Morozova (1931-2021).

1. Introduction

The climate and landscapes repeatedly changed on the East European Plain over the Quaternary period. The changes have been recorded in the natural archives and stored as loess-paleosol sequences (LPSs). Apart from loess and paleosols, the LPS may contain various deposits, such as till or alluvial sands and gravels, etc. (Stremme, 1998; Velichko et al., 2006b; Rusakov et al., 2007; Panin et al., 2019b). The East European Plain is, in fact, one of the largest areas of the loess occurrence (Velichko, 1990; Haase et al., 2007). Here in the loess-paleosol sequences (LPS), there are till deposits left by the Quaternary ice sheets (Velichko et al., 2006a; 2011), which exerted a considerable influence on the environments. The soils that occur on the surface might be distorted or destroyed completely by the oncoming ice sheet (Fitzsimons and Lorrain, 2011; Derbyshire and Owen, 2018). Significant volumes of meltwater formed ice-dammed lakes locally, thus increasing soil erosion (Fitzsimons and Howarth, 2018). With the onset of the warmer period, the glacier melted and left the till that overlies the remains of soils. The

* Corresponding author.
E-mail address: pgpanin@igras.ru (P.G. Panin).

https://doi.org/10.1016/j.catena.2021.105445
Received 15 December 2020; Received in revised form 27 April 2021; Accepted 10 May 2021
Available online 27 May 2021
0341-8162/

paleosols found under till may be compared with the soils in the extra-glacial zone; that gives grounds to determine the soil type and reconstruct their development environments (Retallack, 2019).

Herewith we are considering the Likhvin section (also known as «Chekalin»), where the LPS includes, apart from paleosols and loess horizons, a thick series of till. The Likhvin section was first mentioned by Bogolubov (1904), who described in detail its geological sequence. Further investigations of the section continued (Moskvitin, 1931; 1967; Grichuk, 1950; Ushko, 1959; Sudakova and Aleshinskaya, 1974; Bolikhovskaya et al., 1976; and many others). The sequence includes at least seven paleosols, as many as three horizons of till and five cryogenic horizons; the stratigraphic units yielded palynological spectra (Bolikhovskaya and Sudakova, 1996; Bolikhovskaya and Molodkov, 2006; a. o.), and faunal assemblages (Agadjanian, 1977). Besides, the deposits were dated by thermoluminescence (Faustov et al., 1974; Dobrodeyev and Il'ichev, 1974; Sudakova, 1975) and OSL methods (Little et al., 2002), along with studies of their paleomagnetic characteristics (Faustov et al., 1974), quartz grains studied (Timireva and Velichko, 2006) and composition of humus material of the paleosols (Glushankova, 1971). The thoroughly studied Likhvin section is taken as the stratotype of the Likvin Interglacial (Markova, 2006); since 1977, it is included in the list of specially protected natural objects. The sequence is rather complicated in structure. The paleosol horizons are occasionally interrupted and replaced with lacustrine or glacial deposits, making it difficult to reconstruct climatic changes in the studied region (Pisareva et al., 2019). So the LPS of the Likhvin sequence was analyzed once more using the high-resolution sampling, which had been successfully employed in the LPS studies and the climate reconstructions in Central Europe (Antoine et al., 2009a; Krauß et al., 2016; Moska et al., 2019; Adameková et al., 2021; a.o.), China (Zeng et al., 2017; Wu et al., 2018; a.o.), and in other countries (Tecsa et al., 2020; Lu et al., 2020; a.o.). The high-resolution analysis applied to study in detail the structure of paleosols and more accurately diagnose their type of soil formation, making it possible to reconstruct the climatic conditions in which it developed.

The present research is aimed to study paleosols in the LPS of the Likhvin section using a set of methods: the particle-size distribution, magnetic susceptibility (MS), the loss on ignition values, total organic carbon (TOC), pH, and micromorphology. The configuration of paleosols and the type of their soil formation will make it possible to reconstruct the climatic conditions that prevailed in the Late and Middle Pleistocene in the study area. The new OSL and AMS dates will clarify the paleosols' age and stratigraphic position in the section. The present work is the first experience of the high-resolution analysis applied to the LPS series in that region.

2. Materials and methods

2.1. Regional setting

The studied region is located in the northwest of the Central Russian Uplift (the central part of the East European Plain). As to the regional topography, it features secondary till plains heavily dissected with erosion. The studied region belongs to the area of the ancient glaciation formerly covered with ice sheets (Sudakova and Antonov, 2021). Its temperate continental climate corresponds to the Atlantic continental region (Alisov, 1947) or zone Dfb (Kottek et al., 2006). The mean annual temperature amounts to 5.4 °C on average, the mean temperatures of January and July are −8.5 °C and 19 °C (Bulygina et al., 2015). The moisture supply is sufficient, it amounts to ~ 600 mm on average, while the potential evaporation is about 500–600 mm (Bulygina et al., 2015).

The Likhvin exposure occurs on the left side of the Oka River valley (Fig. 1), at a distance of 2 km northeast from the town of Chekalin. The total thickness of the exposed sequence amounts to ~ 40 m. The valley slopes are heavily dissected with great erosional landforms. Slope processes are also active. The Likhvin exposure was earlier photographed by Bogolubov (1904) and Ushko (1959). A comparison between photographs taken at different time displays changes in the vicinity of the section occurring over time, as seen in Fig. 1S (Supplementary). The choice of studying and sampling exposure was hindered due to the slopes being heavily eroded or overgrown with shrubs. Of the two sites suitable for studies, the section Likhvin-1/18 (1/18 –number of the section / year of the fieldwork) (N 54°06′45′'; E 36°16′06′') exposes Bryansk paleosol (BR) and paleosols of the Mezin soil complex, as well as the upper part of the Dnieper till. Section Likhvin-2/18 (N 54°06′21′'; E 36°15′27′') exposes the lower part of the Dnieper till and older Middle Pleistocene deposits, including the Romny paleosol (ROM) and the Early Kamenka interglacial paleosol (EKAM).

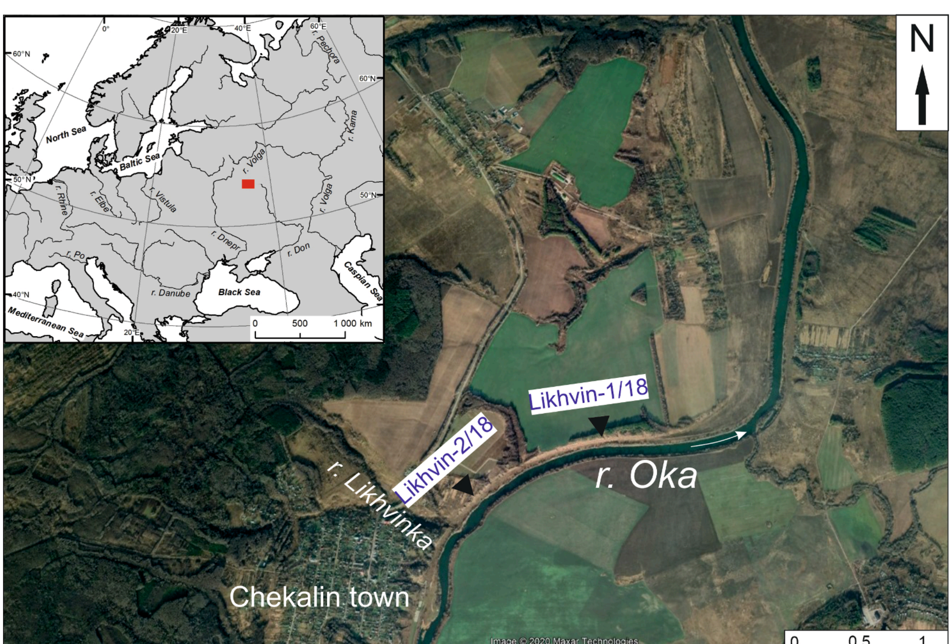

Fig. 1. Geographical position of the sections: Likhvin-1/18 and Likhvin-2/18.

2.2. Field survey

The sections Likhvin-1/18 and Likhvin-2/18 were morphologically described according to FAO (2006). The color of the horizons was determined in the field on a freshly cleared section wall, using the Munsell color system (Munsell Color, 2000). The chronostratigraphy of the Likhvin sequence corresponds to the scheme developed by Velichko and his colleagues (Velichko et al., 2011; Velichko and Morozova, 2015). According to the IUSS Working Group WRB 2014 (2015), the names of the modern soils and paleosols are given.

Linear topographic and geodetic profiling was performed to precise vertical positioning of sections Likhvin-1/18 and Likhvin-2/18, and the construction of the profile across the Oka River valley side. Points of the State Geodetic Network of the Russian Federation were used as the planimetric and altimetric basis. The Global Navigation Satellite System (GPS/GLONASS) «EFT M4» was used in the fieldwork. Fig. 2S displays profiles of the Likhvin section compiled by the earlier investigators (Moskvitin, 1967; Bolikhovskaya et al., 1976; Bolikhovskaya and Sudakova, 1996) and those obtained in the course of our field works.

Bulk samples for analyses of the chemical and physical properties were taken in a loose state from the levels undisturbed by cryogenic or biogenic processes. The sampling was performed continuously with a step of 5–10 cm intervals, except for layer 17 (section Likhvin-1/18). The undisturbed samples for micromorphological analyses were taken with sufficient details permitting a thorough description of soil horizons and enclosing sediments. Also, samples have been taken from the cryogenic wedges to estimate soil microstructure changes due to cryogenesis.

Samples for radiocarbon dating have been taken from the modern soil (Bt horizon) and Ag horizon of the Bryansk paleosol (BR). In 2018, seven samples for OSL dating were taken from Likhvin-1/18 section (field code № L1-L7 in Table 1S) and two more – from section Likhvin-2/18. In 2020, additional sampling was performed from layers 8 and 10, section Likhvin-1/18 (field code № Likhvin 1 and Likhvin 2). The samples for OSL were taken after the wall had been cleaned to a depth of 10 cm using steel tubes 50 mm in diameter and 250 mm long. The analysis of Dnieper till deposits was not included in the objectives of this study. See the sampling locations for AMS, OSL, and bulk samples in Fig. 2. Samples taken for micromorphological studies are shown in Fig. 3.

2.3. Laboratory analyses

A total of 245 bulk samples (sections Likhvin-1/18 and Likhvin-2/18) were analyzed using standard laboratory analytical methods that are used in modern soil science (FAO, 2006): particle size distribution, the total organic carbon, and pH measurements. To distinguish paleosol levels in the loess (Hou et al., 2020; Zykina et al., 2020; Liu et al., 2021; a.o.), especially humus horizons, the following methods were additionally used: the loss on ignition, the magnetic susceptibility, and color.

A laser diffraction analyzer Malvern Mastersizer 3000 with Hydro EV sample dispergator was applied to measuring particle-size distribution using a Fraunhofer approximation. The bulk sample preparation included the following steps: pouring in 10% solution of HCl acid for 24 h; treated with a ~30% solution of hydrogen peroxide H_2O_2 until the reaction stops; deflocculating the material by a 4% solution of tetrasodium pyrophosphate $Na_4P_2O_7$ and then additional dispersion of clay aggregates by ultrasound (40 W max, 40 kHz for 100 s in Hydro EV dispergator before the measurement). GRADISTATv8 software (Blott and Pye, 2001) was applied for the calculation of grain size statistics. When describing the soil characteristics, the 2000–63–2 μm system was used as given in FAO–ISRIC (1990).

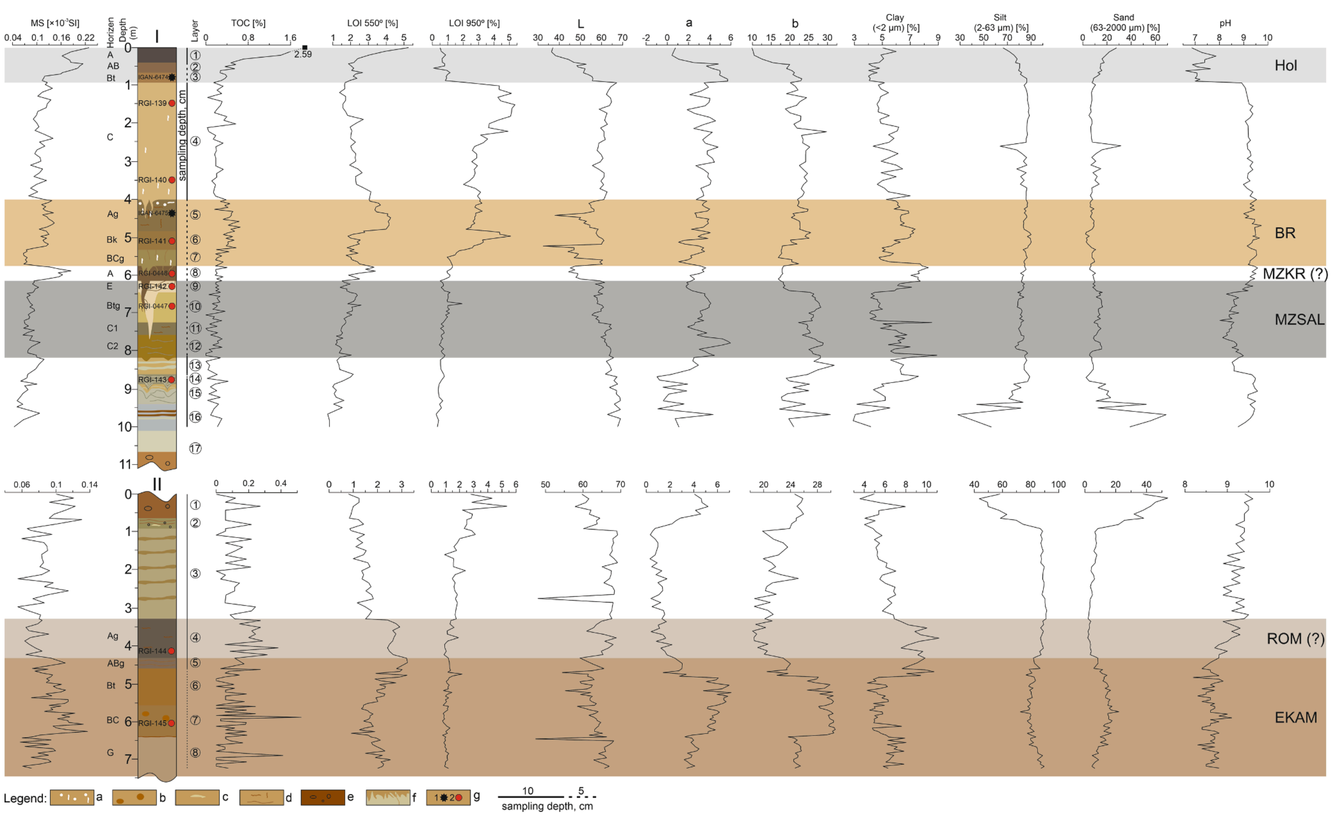

Fig. 2. Physico-chemical and MS properties of Likhvin-1/18 (I) and Likhvin-2/18 (II) sections. Legend: a – carbonate pedofeatures; b - mole burrows; c - sandy interlayers; d - Fe interlayers; e - inclusions of pebbles, gravel; f – cryogenic wedges and fissures of different genesis; g – sampling locations AMS (1) and OSL (2) dates. TOC [%] - organic carbon; LOI [%] - loss on ignition; Color parameters (L, a, b). See Supplementary data. Hol – modern soil (Holocene); BR - Bryansk paleosol; MZKR - Krutitsa interstadial paleosol; MZSAL - Salyn interglacial paleosol; ROM - Romny paleosol; EKAM – Early Kamenka interglacial paleosol.

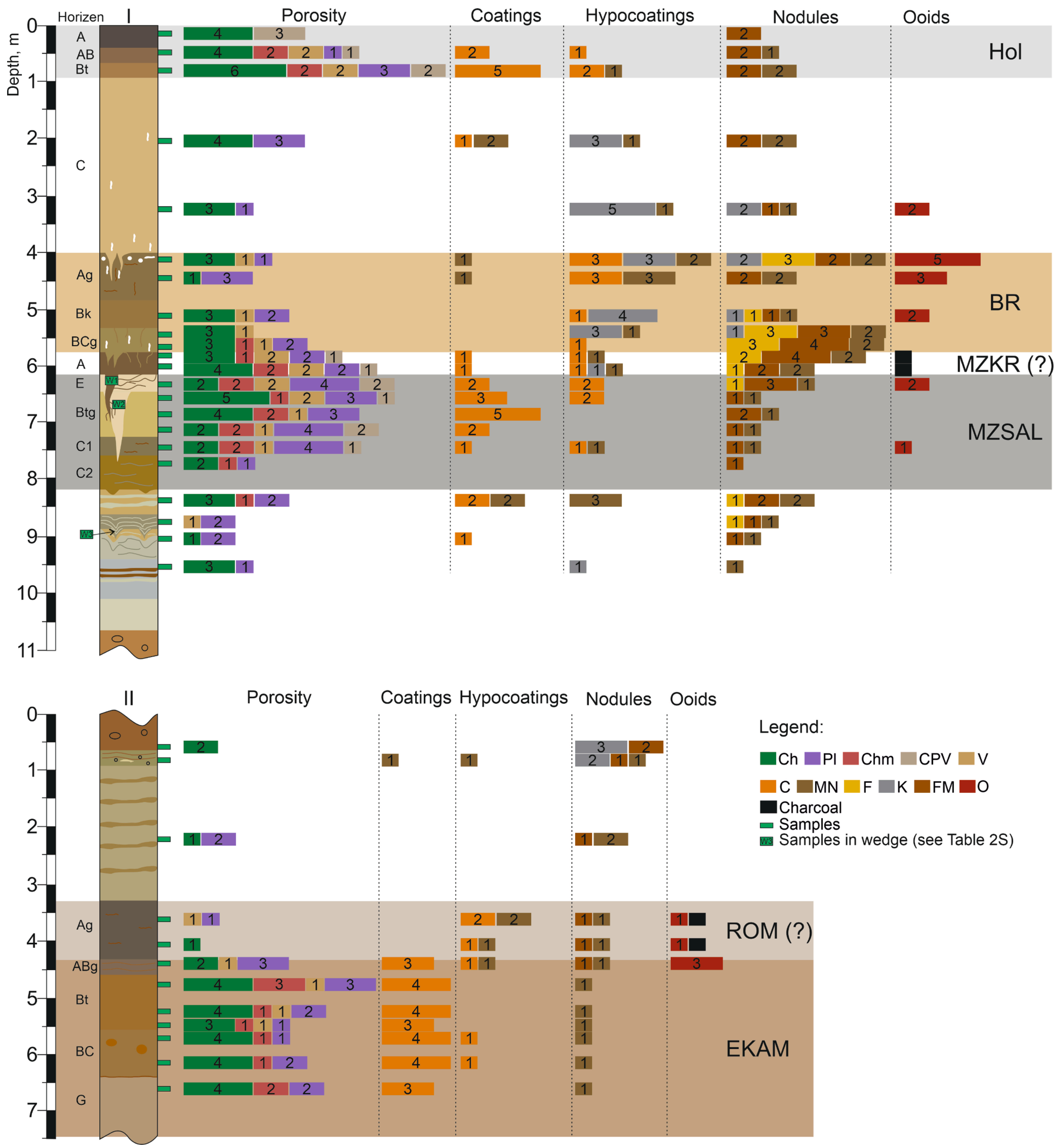

Fig. 3. Micromorphological characteristics of Likhvin-1/18 (I) and Likhvin-2/18 (II) sections. Ch - channels, Pl — planes, Chm — chambers, CPV – compound packing void, V — vugh, C — clayey material, MN – Mn material; F - Fe material; K – carbonate material; FM – Fe-Mn material; O – ooids; Samples – places of sampling for micromorphological analysis. See legend Table 2S.

The total organic carbon (TOC) was determined by the Tyurin method: first, organic debris (roots, seeds, charcoals) had been removed from the pre-dried samples; then they were ground to a state of powder, and the average sample weighing 50–100 mg depending on its color was taken. The soil bulk sample size depends on the estimated TOC content as indicated by the color of the soil. The amount of TOC is determined by the wet ashing of organic compounds of the soil with a chromium mixture. The process is based on the oxidation of soil organic carbon by 0.4 N potassium dichromate solution ($2K_2Cr_2O_7$), prepared with sulfuric acid in a ratio of 1:1. The oxidation reaction of organic carbon with a chromium mixture proceeds according to the equation: $2K_2Cr_2O_7 + 8H_2SO_4 + 3C$ (organic carbon) $= 2Cr_2(SO_4)_3 + 2K_2SO_4 + 8H_2O + 3CO_2$. The TOC content is determined by the amount of chromium mixture consumed for the oxidation of organic matter. Ashing is carried out in heat-resistant flasks with a volume of 100 ml. At the end of the ashing, the liquid in the flask should have a brownish color. If it has a bright green hue, this means that during the ashing process, all the dichromate was reduced to trivalent chromium ions, which have an intense green color, and there was not enough of it for ashing organic carbon. In this case, the experiment should be repeated while reducing the amount of soil. After cooling the bulk sample, the excess chromium mixture is titrated with Mohr's salt ($6FeSO_4(NH_4)_2SO_4$). The reaction of the rest of the mixture proceeds according to the equation: $6FeSO_4(NH_4)_2SO_4 + K_2Cr_2O_7 + 7H_2SO_4 = Cr_2(SO4)_3 + 3Fe_2(SO4)_3 + 6(NH_4)2SO_4 + K_2SO_4 + 7H_2O$. Phenylanthranilic acid solution is used as an indicator. The difference between the amount of Mohr's salt that was used to titrate the chromium mixture in the experiment without soil (control) and the experiment with soil determines the amount of Mohr's salt in ml, which corresponds to the TOC content of the bulk sample (Arinushkina, 1970). Calculation of the results of determining TOC (%) is carried out according to the equation: TOC=((a-b)·H·0.003)/m)·100, where is: a - the volume of Mohr's salt used for titration in determining the concentration of dichromate solution, ml; b - the volume of Mohr's salt used for titration of the chromium mixture after combustion of the sample, cm; H - concentration of Mohr's salt; 0.003 – the mass of carbon in the reaction, g; m – dehydrated bulk sample of soil, g. For each bulk sample, the content TOC was determined twice.

pH values were measured by HI 98127 (Hanna Instruments, Woonsocket, RI, USA) pH-tester in the water solution of the soil sample (proportion 1:2.5) (Arinushkina, 1970).

The method developed by Heiri et al. (2001) for measurement of the loss on ignition (LOI) implies drying and igniting the bulk samples in the muffle furnace at 105 °C for 12 h (to measure the dry weight), then at 550 °C for 4 h (so that the organic matter turns into carbon dioxide and ash) and then at 950 °C for 2 h (carbon dioxide is evolved from carbonate leaving oxide). The weight was measured after every ignition by the electronic scale. The resulting values are calculated by formulas as follows: LOI550°C=((DW105-DW550)/DW105)·100 and LOI950°C=((DW550-DW950)/DW105)·100, where DW is the dry weight. LOI 550 °C value represents organic matter content, and LOI 550 °C - LOI 950 °C values mean the loss of CO_2 from carbonates.

The magnetic susceptibility (MS) was measured using SM-30 kappameter (ZH instruments, Brno, Czech Republic). Every sample was measured four times, and the mean value was calculated.

The CS-10 (Hangzhou CHNSpec Technology Co., Ltd., Hangzhou City, China) 8 mm instrument – portable digital colorimeter – was used for color measurements. The bulk samples were previously dried at 20 °C for two weeks and then ground in a mortar to a state of smooth powder. A weighed portion of ~ 5 g was placed in an opaque cuvette, and the surface was smoothed. The instrument was positioned perpendicular to the surface of the sample-bearing cuvette to perform the measurements. The color of each bulk sample was measured three times. The data thus obtained is expressed in the coordinates of the CIELAB color space (L, a, b).

The paleosol microstructure was studied in thin sections less than 30 μm thick. In the preparation of a thin section 2.5 × 4 cm in size, the polysynthetic resins were used under vacuum impregnation conditions. The thin sections were studied under the microscope Zeiss Axio Scope. A1 at 2.5x/0.085 Pol (∞/0,17) magnification. The soil-forming processes and their quantitative characteristics were interpreted as described in the literature (Stoops, 2003; Stoops et al., 2010). The total number of the analyzed thin sections amounts to 37, three of them having been taken from cryogenic wedges.

The radiocarbon dates were obtained using the Accelerator Mass Spectrometry (AMS) technique at the Center for Collective Use, Laboratory of Radiocarbon Dating and Electronic Microscopy, Institute of Geography Russian Academy of Sciences (IGANAMS index). The preparation of all samples for AMS (i.e., the preparation of samples and the separation of datable fraction, graphitization, pressing on a target) was performed in the Institute of Geography RAS. The automated AGE-3 graphitization system (Ionplus) was applied to graphitization. Graphite 14C/13C ratios were measured using the CAIS 0.5 MeV accelerator mass spectrometer at the Center for Applied Isotope Studies, University of Georgia (USA). The results were calibrated using the radiocarbon calibration program CALIB REV7.1.0 (Stuiver and Reimer, 1993) with the calibration dataset Intcal13 (Reimer et al., 2013).

Nine OSL samples were dated (Table 1S) using both quartz (9 samples) and K-rich feldspar (2 samples). All measurements were conducted at the OSL Laboratory of A.P. Karpinsky Russian Geological Research Institute (St. Petersburg, Russia). The standard method (e.g. Wintle, 1997) was applied to prepare the samples, resulting in selecting quartz and K-rich feldspar grains in the sand size fractions 180–250, 90–180 and 63–90 μm. The optically stimulated luminescence (OSL) measurements were undertaken using a Risø TL/OSL Reader DA-20C/D (Lapp et al., 2015) on stainless steel discs. Blue light stimulation ($\lambda = 470$ nm, ~100 mW cm^{-2}) and photon detection through a 7.5-mm Hoya U-340 glass filter was applied for quartz, infrared stimulation ($\lambda = 870$ nm, ~175 mW cm^{-2}) and photon detection through a Schott BG39/BG3 filter combination (2 and 3 mm, respectively) was applied for K-rich feldspar. A beta irradiation $^{90}Sr/^{90}Y$ source was used to irradiate samples. It was calibrated for discs and cups using Risø 180–250-μm calibration quartz (Hansen et al., 2015).

The equivalent doses (D_e) in quartz were estimated employing the SAR protocol (Murray and Wintle, 2000; 2003), whereas the D_e estimates in feldspar were done using the post-IR IRSL ($pIRIR_{290}$) SAR protocol (Thiel et al., 2011). The OSL IR depletion ratio (Duller, 2003) was measured in three quartz aliquots of every sample. If the ratio was less than 90%, samples were additionally etched with 40% HF. The combined preheat plateau and dose recovery test was carried out to evaluate SAR protocol suitability for quartz and assess an applicable preheat temperature. A plateau was observed at preheating temperatures 160–240 ℃. The average measured-to-given ratio is 1.05 ± 0.02 (n = 36). A primary analysis of OSL data was done using the Analyst software package (Duller, 2015). The OSL signal was summed over the initial 0.32 s less than from the subsequent 0.8 s for quartz. The $pIRIR_{290}$ and IR_{50} equivalent doses in K-rich feldspar were obtained by summing the first 0.8 s less the last 10 s. The quartz and K-rich feldspar's dose–response curves were fitted with a sum of two exponential functions or an exponential function with a linear component. We applied the arithmetic mean to calculate the final D_e values presented in Table 1S. Individual aliquot D_e values, which had the relative uncertainty exceeding 30%, were rejected. The interquartile range was used to find outliers in data.

The environmental radionuclide activities of ^{238}U, ^{226}Ra, ^{232}Th and ^{40}K were measured applying a high-resolution gamma spectrometer (Murray et al., 1987) with high purity germanium (HPGe) radiation detector Canberra BE3825. The samples had been sealed by wax in plastic cups and kept for at least 20 days before measurement to allow ^{222}Rn to reach equilibrium with its parent ^{226}Ra. The activities were converted to the infinite matrix dose rates using the conversion factors of Liritzis et al. (2013). We assumed that the sediments' average burial water content was around 75% of saturated water content. The internal beta dose rates in K-rich feldspar were calculated based on K concentration 12.5 ± 0.5% (Huntley and Baril, 1997) and Rb concentration 400 ± 100 ppm (Huntley and Hancock, 2001). The internal alpha dose rates in K-rich feldspar and quartz were estimated as 0.10 ± 0.05 Gy ka^{-1} (Mejdahl, 1987) and 0.010 ± 0.002 Gy ka^{-1} (Vandenberghe et al., 2008), respectively. The contribution from cosmic rays to the dose rates was calculated according to Prescott and Hutton (1994) using the current burial depths. The OSL ages were derived by dividing the average equivalent doses by the total dose rates.

3. Results

3.1. Morphology

The modern soil, as described in Likhvin-1/18 section (see Fig. 4) is classed with Phaeozems, with typical profile A-AB-Bt-C (Fig. 4–1a). The horizon A at a depth of 0–0.4 m is dark-grey in color (2.5Y4/2) granular silty loam, with distinct wavy boundary, slightly moist, includes

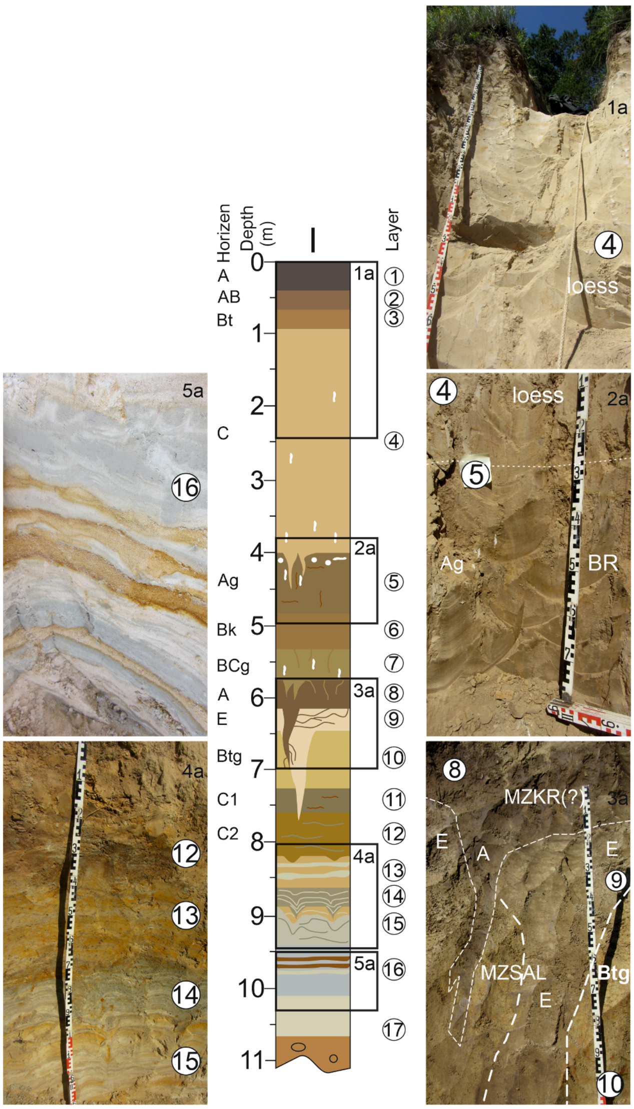

Fig. 4. Morphology of Likhvin-1/18 section. 1a – loess horizon C (layer 4); 2a - the horizon Ag of the Bryansk paleosol (BR) (layer 5) under loess horizon C (layer 4); 3a - paleosols of the Mezin soil complex with pronounced cryogenic wedges (MZSAL - Salyn interglacial paleosol (layers 9–10), MZKR - Krutitsa interstadial paleosol (layer 8)); 4a - series of layers under the Mezin soil complex; 5a - alluvial deposits composed of homogeneous blue-grey loamy sand alternating with whitish and brown sand. See Fig. 2 for the legend for the section column. (For interpretation of the references to color in this figure legend, the reader is referred to the web version of this article.)

occasional roots. AB horizon (0.4–0.65 m) is dark brown with greyish hue (10YR4/4), similar in appearance to A horizon; low bleached sandy spots appear downward, the transition is gradual. Bt horizon (0.65–0.95 m) is brown (10YR5/4) silt, granular and blocky subangular, with a few mottles of organic, pseudomycelia, with wavy boundary and abrupt transition. Horizon C (loess) (0.95–4.0 m) is pale yellow silt with brownish hue (2.5Y7/4), includes Fe-Mn concretions, pseudomycelia, fine voids are common, blocky subangular structure, hard carbonate concretions, moderately calcareous.

The BR paleosol profile displays sighs of gleying and consists of horizons Ag-Bk-BCg (Fig. 4-2a). Ag horizon (4.0–4.8 m) is blue-grey, with a brownish hue (2.5Y6/4), slightly moist, with Fe-Mn concretions. The horizon is penetrated with cryogenic wedges to a depth of 10–15 cm filled with yellowish material from the overlying C horizon. There are hard carbonate concretions 1–1.5 cm in diameter and 6 cm long concentrated in the Ag horizon's upper part. Ferruginous interlayers 1–2 mm thick occur occasionally. The lower-lying Bk horizon (4.8–5.3 m) is brown (2.5Y6/6), with rare fine voids and blue-grey spots of gleying 1–2 mm in diameter; the transition is abrupt. BCg horizon (5.3–5.7 m) is bluish-grey with brownish hue (2.5Y6/4), Fe-Mn concretions; there are noticeable old root channels up to 3 mm in diameter, filled with carbonate material. Fissures 2–3 cm wide penetrate the horizon from the top to a depth of 5 cm; they are filled with the B horizon material.

Below the BR, there are two paleosols of the Mezin soil complex (Fig. 4-3a). The upper paleosol is present as A horizon; in the opinion of A.A. Velichko (Little et al., 2002), it is correlatable with the Krutitsa interstadial paleosol (MZKR). This A horizon (5.7–6.1 m) is dark-grey (10YR4/2) irregularly colored silt, slightly moist, blocky subangular. The horizon is broken with wedges and fissures reaching the depth of 25 cm and filled with the material of BCg horizon of the BR. The lower paleosol – the Salyn interglacial paleosol (MZSAL) presents E-Btg-C1-C2 profile. The upper horizon – E (6.1–6.45 m) is blue-grey silt with a brownish hue (10YR5/2), slightly moist. The horizon is broken with a wedge filled with humified material and penetrating from A horizon of the MZKR paleosol. Some horizontal humified interlayers up to 1 cm thick are also recorded. The Btg horizon (6.45–7.25 m) is brown with a bluish hue (2.5Y6/4), granular, with Fe concretions, and a few mottles of organics. The horizon is penetrated with two wedge structures. One of them is filled with humified matter from A horizon of the MZKR, and the other penetrates from the overlying E horizon. C1 (7.25–7.55 m) and C2 (7.55–8.15 m) horizons are gleyed, abound with Fe-Mn and Mn concretions, the lower C2 horizon is cryoturbated.

Layers 13–14 (Fig. 4-4a) – alluvial deposits, floodplain facies – represent a series of stratified loam and sandy loam. In common with the underlying horizon, blue-gray (5Y6/2) loam interlayers alternate with whitish (2.5Y7/3) and brown (2.5Y6/8) layers bearing traces of ferrugination. Layers 15–16 (Fig. 4-4a, Fig. 4-5a) are also attributed to alluvial deposits, floodplain facies; those are stratified series of sand and sandy loam (interlayers are 5 to 10 cm thick), composed of homogeneous blue-grey loamy sand (5Y5/2) alternating with whitish (2.5Y7/2) and brown sand (2.5Y6/8). The stratification is more conspicuous due to ferrugination. The upper part of the horizon bears traces of ice-wedge pseudomorphs – two small-scale wedges (26 × 10 cm in size, with a distance of 30 cm between wedges). They are filled with material from the above-lying layer (Fig. 4-4a). Layer 17 presents the uppermost part of the Dnieper till overlain with sand deposits.

The Likhvin-2/18 begins with layer 1 represented by the Dnieper till (Fig. 5-1b) – that is sandy clay (loam) with pebble (5–10 cm); the layer is dark red with a brownish hue (7.5YR4/6), with interbeds and lenses of light-colored sand (10YR5/4). According to the earlier investigators (Yakovleva, 1956; Pisareva et al., 2019), the Dnieper till consists of three layers and includes fragments of rocks brought from eastern Karelia and the Onega Lake region. The uppermost series of the boulder loam is dominated by crystalline rocks, while the lowermost one includes mostly sedimentary rocks (Karpukhin and Lavrov, 1974). The layer between those of boulder loam is composed of sand and gravel. The long axes of rock fragments in all three till layers are oriented in a submeridional direction with a slight deviation to the northeast. The three-layer series of the glacial deposits varies in thickness from 6 to 7 to 17 m within the section (Bolikhovskaya et al., 1976; Sudakova and Bol'shakov, 1977; Pisareva et al., 2019).

Layer 2 is a transitional assimilatory horizon including the rocks of the former glacier substrate and stratified clay loam; the latter presents alternating interlayers of brown (2.5Y5/4) and blue-grey (2.5Y5/2) colors varying in thickness, with Fe-Mn smears and Fe smudges. Small lenses of sand occur locally, and inclusions (up to 10%) of small pebble and gravel (less than 1 cm). Layer 3 (Fig. 5-2b) consists of homogeneous silt of blue-grey (5Y7/3) color with light brown interlayers. In earlier authors' opinion (Sudakova and Bol'shakov, 1977; Bolikhovskaya and Sudakova, 1996; Pisareva et al., 2019; a.o.) layer 3 has been interpreted as loess-like deposits formed in the ice-dammed basin at the time of the

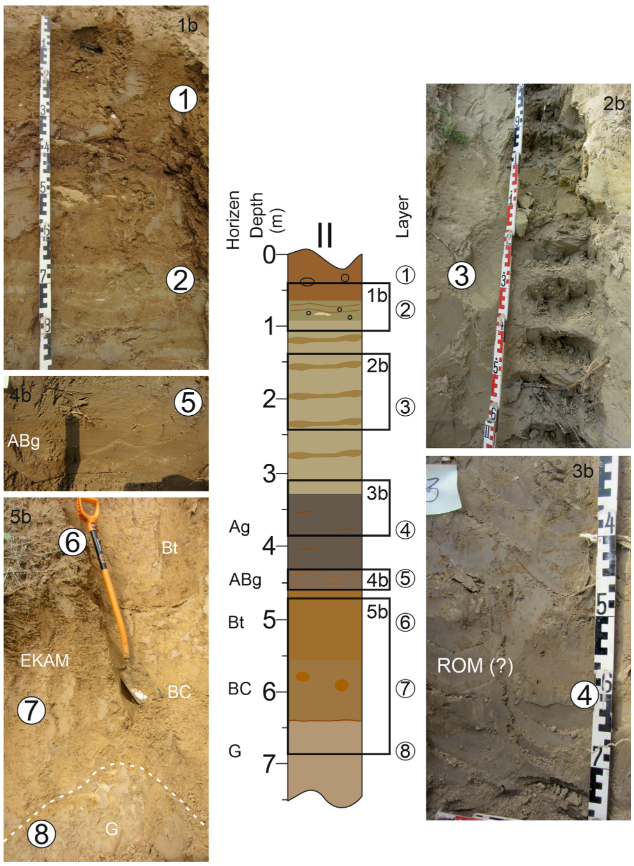

Fig. 5. Morphology of Likhvin-2/18 section. 1b - the lower part of the Dnieper till (layer 1) and the underlying layer 2; 2b - deposits of layer 3; 3b – the horizon Ag (layer 4) of the assumed the Romny paleosol (ROM); 4b - the horizon ABg (layer 5) of the Early Kamenka interglacial paleosol (EKAM); 5b - the soil crossover of the Early Kamenka interglacial paleosol. See Fig. 2 for the legend for the section column.

Dnieper ice sheet advance.

There is a horizon of soil formation traceable at a level of layer 4 and correlatable with ROM (Romny paleosol, see Little et al., 2002). That paleosol (ROM) is present in the section Likhvin-2/18 (Fig. 5) as the humus Ag horizon (3.25–4.35 m). It shows signs of gleying, with a blue-grey hue (2.5Y5/4), abounds in Fe-Mn concretions, thin partings of Fe, blocky subangular, and platy when dry.

The ROM paleosol is underlain with the Early Kamenka interglacial paleosol (EKAM) with profile ABg-Bt-BC-G (Fig. 5-4b; Fig. 5-5b). The uppermost ABg horizon (4.35–4.55 m) (Fi. 4S-4b) is blue-grey (2.5Y5/4), stratified, with brown horizontal ferruginous interbeds less than 1 cm thick. The underlying Bt horizon (4.55–5.55 m) is brown with a bluish hue (10YR5/6), from the depth of 25 cm – brown (7.5YR5/6); it is granular and blocky subangular, with a few mottles of organics, rare fine voids, gradual transition. BC horizon (5.55 – 6.45 m) is brown with a bluish hue (10YR6/6); two mole holes 10 to 20 cm in diameter are filled with brown material, the dark-grey humified coating is traceable at the hole margins. At the lower boundary of the horizon, there is a ferruginous secondary layer 5 cm thick, with whitish lenses of loamy sand. G horizon (6.45–7.25 m) is blue-grey (2.5Y6/4), gleyed, with numerous concretions of Fe-Mn and Fe in composition.

3.2. *Physical-chemical properties and magnetic susceptibility*

The maximum content of clay fraction (8.88%) in the section Likhvin-1/18 is confined to the lower part of C2 horizon, isolated peaks being traced in C1 horizon (8.52%) and the upper part of A horizon of the MZKR (8.27%). As to section Likhvin-2/18, the maximum proportion of the clay fraction (<2 μm) is found in the gleyed ROM (11.02%) and in the upper part of the illuvial Bt horizon (10.56%), see Supplementary 1. As seen in Fig. 2, this fraction is accumulated in the surface or near-surface horizons of the modern soil and paleosols. Its values gradually decrease downwards in the horizons C (modern soil, loess), BCg (BR), Btg (MZSAL), Bt and BC (EKAM). The silt fraction is evenly distributed along the entire Likhvin-1/18 sequence, except for its lower part (layers 15–17) where its proportion decreases sharply. The same is true of the silt fraction distribution over most of the section Likhvin-2/18, except the till layers where it drops conspicuously (Fig. 2). The layers richest in sand proportion are confined to the alluvial deposits overlying till; the paleosol enriched in sand particle proportion is the EKAM.

The highest content of TOC is typical of the humus horizon in the modern soil (2.59; 1.63; 1.45%), next richest is Ag horizon of the BR – 0.67%, further goes A horizon of the MZKR – 0.41%, Ag horizon of the ROM – 0.39%, and ABg horizon of the EKAM – 0.17% (see Fig. 2, and Supplementary 1). The sequence is confirmed by the LOI 550° graph showing the presence of organic matter. Contrary to that, high values of LOI 950° are typical of horizons devoid of distinct signs of the humus matter presence. Such horizons are mostly rich in carbonates, which is confirmed by the pH values. The modern forest soils – Phaeozems – are noted for lower pH values, while the carbonate loess (C horizon) is noted for a sharp rise of pH (Fig. 2). Lower values of pH are typical also of the MZSAL and EKAM paleosols. MS (magnetic susceptibility) measured in the studied sections indicates clearly the levels of humus horizons, including that of the modern soils (0.23), the BR (0.144), and the MZKR (0.185). Other paleosols show much lower MS values (0.093 in the ROM and 0.057–0.143 in the EKAM).

The lightness coefficient «L» in the section Likhvin-1/18 is less than 60 in the modern soil, in the BR, and in the MZKR, the latter being most dark-colored in the section (Fig. 2). The loess C horizon and the MZSAL show «L» values above 60. In the section Likhvin-2/18 «L» values are high and indicate rather light coloration of the lower-lying ROM and EKAM paleosols. The redness coefficient «a» increases insignificantly in the lower horizons of the modern soil and the MZSAL, being lowered in the loess C horizon and layers 1–3 of the section Likhvin-2/18. The maximum «a» values are typical of the EKAM (>6). The yellowness coefficient «b» generally grows from younger to older soils and reaches its maximum in the EKAM.

3.3. *Micromorphology*

The paleosols and loesses studied in considered sections are considerably variable in microstructure (Fig. 3; Table 2S). The paleosols are porous, mostly with channel and plane pore types, with clay coatings concentrated inside. Most abundant clay coatings are found in Bt horizon of the modern soil and Btg horizon of the MZSAL. Coatings are uniformly distributed over the EKAM profile, while the modern soil and the MZSAL display signs of the eluvial-illuvial process. Clay coatings are absent from the gleyed BR; their place is taken by carbonate hypocoatings and numerous nodules of Fe, Fe-Mn and Mn composition. Loess horizons are less abundant in pores; the intra-ped mass is mostly compact and silty. Calcareous hypocoatings and nodules are found in abundance. Charcoals of plant remains are found in the MZKR and ROM microstructure, seemingly absent from other paleosols and loess.

3.4. *Optically stimulated luminescence (OSL) and accelerator mass spectrometry (AMS) dating*

The fast component of a quartz OSL decay curve is preferable for OSL dating since it is most easily reset and is stable over geological time scales (Murray and Wintle, 2000). To check if our quartz samples are dominated by the fast component, we compared the averaged natural OSL decay curve from Likhvin quartz with the averaged OSL decay curve from Risø calibration quartz (Fig. 6) which is known to be dominated by

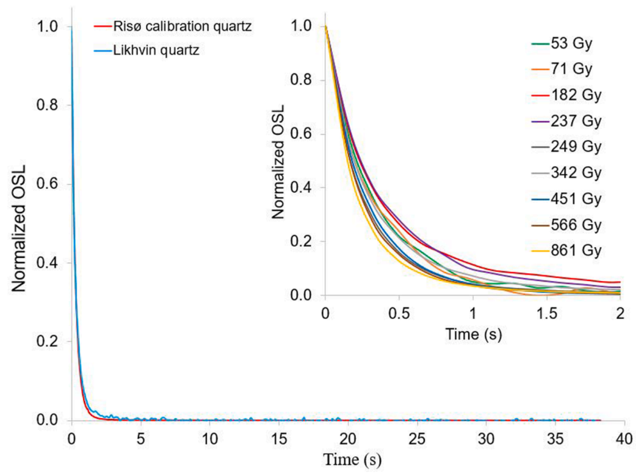

Fig. 6. Comparison of the averaged (n = 9, one aliquot from every sample) natural OSL decay curve from Likhvin quartz with the averaged (n = 6) OSL decay curve from Risø calibration quartz. Inset shows a comparison of natural OSL decay curves from Likhvin quartz corresponding to different De values. All OSL stimulation curves were normalized and background subtracted.

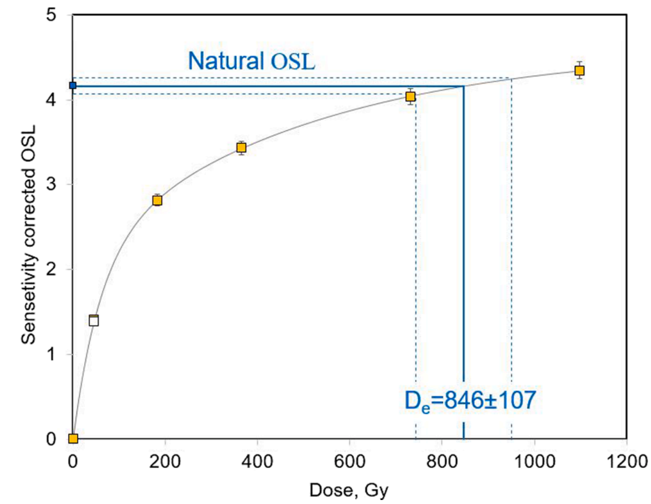

Fig. 7. Typical quartz dose–response curve of a single aliquot from the sample RGI-145 (the open symbol represents the recycling point).

the fast component (e.g. Jain et al., 2003). It is clear from the Fig. 6 that the OSL decay curves are almost identical, so we can infer that Likhvin quartz is dominated by the fast component and it is suitable for OSL dating. Inset in Fig. 6 shows that the shape of a natural OSL decay curve does not have a strong dependence on the corresponding D_e value. It means that all our samples have similar luminescence characteristics which are suitable for OSL analysis. A variety of studies undertaken over the recent years using quartz grains from samples with independent age control (e.g., Buylaert et al., 2007; Lai, 2010; Timar-Gabor et al., 2011) prove age underestimation when the paleodoses are higher than 100–200 Gy. On the other hand, in some cases (e.g., Watanuki et al., 2005; Murray et al., 2008; Nazarov et al., 2020), quartz ages in good agreement with expected values were received based on equivalent doses higher than 200 ka. Our study obtained quartz equivalent doses higher than 100 Gy for 7 samples (Table 1S). The OSL dates obtained on quartz from the loess (C horizon) – 17.9 ± 1.1 and 27.7 ± 1.9 ka are correlatable to MIS 2. In layer 6 of the Likhvin-1/18 section, the OSL analysis showed the date 67 ± 7 (on quartz), which corresponds to the MIS 4. The ages of samples RGI-446 and RGI-447 having D_e values 209 and 288 Gy respectively are in good agreement with the K-rich feldspar ages (average ratio of KF/Q = 1.03 ± 0.6, n = 2). Thus, we can conclude that our quartz ages are reliable at least when the equivalent doses lower than 300 Gy. According to OSL dates (86 ± 6 ka (on K-rich feldspar, protocol - pIRIR290 SAR) and 88 ± 6 ka (on quartz)), the sediments of the MZKR paleosol correspond to MIS 5a and 5b. In the underlying layer 9, OSL date – 86 ± 6 ka (on quartz) is also correlated with MIS 5b. In the middle part of horizon Btg (layer 10) of the MZSAL paleosol, the obtained dates 118 ± 8 ka (on K-rich feldspar, protocol - pIRIR290 SAR) and 108 ± 11 ka (on quartz) indicate MIS 5e and 5d.

Two quartz samples RGI-144 and RGI-145 (S), have equivalent doses higher than 300 Gy. Corresponding dose–response curves dose do not saturate even at 1000 Gy (Fig. 7), which is why the finite ages were obtained for these samples (148 ± 18 ka; 283 ± 44 ka). Unfortunately, we cannot confirm the reliability of these dates in the framework of this study, so we give the infinite ages (>119 ka; >112 ka) that are more reliable as well (S). The ages of all but one RGI-143 (S) of the samples are close to expected values.

The AMS dates (Table 3S) also correspond to the time intervals in which the modern soil – 5164 cal BP (Holocene) and the BR paleosol – 29987 cal BP (MIS 3) were formed.

4. Discussion

4.1. Paleopedogenesis

The paleosols studied in sections Likhvin-1/18 and Likhvin-2/18 developed in different environments and climates. According to the paleosol genesis and zonality and taking into consideration their differentiation into genetic horizons, the paleosols are separated into interglacial and interstadial ones (Velichko and Morozova, 2015). In the section under discussion, the BR, the MZKR, and the ROM are considered to be interstadial, and the MZSAL and the EKAM are attributed to interglacial soils (Little et al., 2002). Interglacial and interstadial paleosols in LPS generally occur close to each other and form soil complexes (Velichko et al., 2007; Panin et al., 2018). So in the chronostratigraphic scheme by Velichko et al. (2011), the soil complexes are represented by the early interglacial phase of the soil formation and the subsequent interstadial phase. For example, the Kamenka soil complex consists of the Early Kamenka interglacial paleosol (EKAM) and Late Kamenka interstadial paleosol (LKAM); the same is the case of the Mezin soil complex, except the terms “late” and “early” are not applied to the soil names. The Bryansk (BR) and Romny (ROM) paleosols do not form complexes, so according to the stratigraphic scheme by Velichko et al. (2011), they are considered to be individual levels of soil formation belonging to MIS 3 and MIS 6, respectively.

4.1.1. The Bryansk paleosol (BR)

The BR paleosol (layers 5–7) of the Likhvin-1/18 section is one of the Late Pleistocene paleosols. It’s well pronounced in the LPS over most East European Plain territory (Morozova, 1981; Velichko, 2002; Sedov et al., 2016; Panin et al., 2018, 2019a; Sycheva et al., 2019; a.o.). The soil profile of the BR is distinctly recognizable in the section due to the bluish hue indicative of the gleying processes. The processes are confirmed by the presence of Fe-Mn pedofeatures in the paleosol at the macro- and microlevel (Fig. 8a, b) (Zaidelman, 1974; Vepraskas et al., 2018; a.o.), as well as by more significant clay proportion (Fig. 2). The high values of LOI 550° correspond to the presence of organic matter in Ag horizon (layer 5) typical of the humus-accumulative horizons of the modern soil. Earlier Morozova (1981) had noted a presence of rounded aggregates – ooids – in the BR microstructure (Fig. 8c), presumably resulting from cryogenic processes (Van Vliet-Lanoë, 1998; Nejman et al., 2017). In the considered case, the maximum concentration of those aggregates is typical of the surficial Ag horizon (layer 5) and decreases downwards (Fig. 3). The presence of carbonate macro-concretions in Ag horizon (layer 5) is related to secondary pedogenic

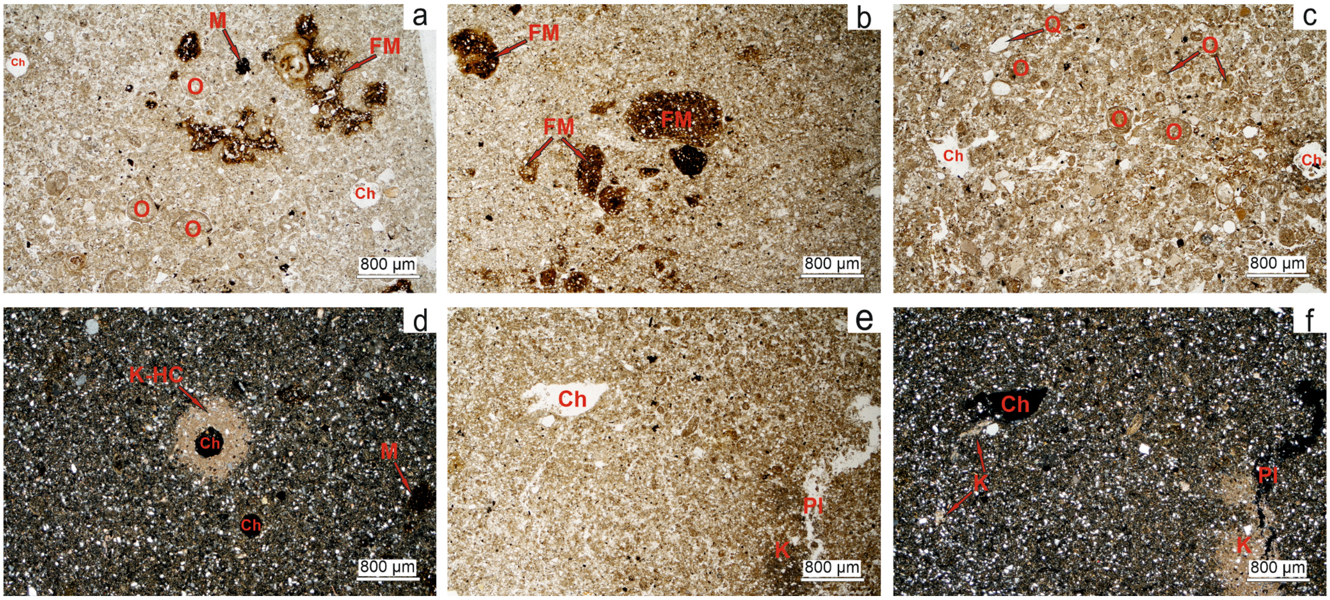

Fig. 8. Microstructure of the BR: a (PPL), c (PPL), d (XPL) - the horizon Ag; b (PPL) - the horizon BCg; e (PPL), f (XPL) - the horizon Ag. Legend: Ch - channels, Pl — planes, K – carbonate nodule; M – Mn nodule; FM – Fe-Mn nodule; K-HC – carbonate hypocoating; Q – quartz; O – ooids.

processes. Due to the clayey composition of the BR, the subsoil water stagnated at the transition between the paleosol and loess, which resulted in large-size concretions (Zamanian et al., 2016) and hypocoatings (Fig. 8d) (Durand et al., 2018). Simultaneously, poorly developed calcareous nodules are less than 150 µm in diameter (Fig. 8e, Fig. 8f). Quite possibly, those are primary carbonates that did not dissolve completely during the soil formation.

The gleying processes are only poorly pronounced in the lower-lying Bk horizon (layer 6). The proportion of Fe and Fe-Mn pedofeatures in its microstructure drops conspicuously; the horizon color becomes more brownish, as indicated by the lightness «L» and yellowness «b» coefficients (Fig. 2). The distribution graphs of the TOC, MS, and the clay fraction made a connection between Bk (layer 6) and Ag (layer 5) horizons; no abrupt change is traceable. A distinct differentiation is seen at the level of BCg horizon (layer 7). Quite possibly, the principal soil processes in BR are related to Ag-Bk profile (layers 5, 6), while BCg horizon (layer 7) is actually a layer of soil-forming loess (that is, parent rock for soil) deposited at an earlier stage of MIS 3. That is supported by LOI 550° and LOI 950° graphs (Fig. 2), which indicate an eluvial-illuvial distribution of carbonates within Ag (layer 5) and Bk (layer 6) horizons. There are fissures (Fig. 2) within BCg (layer 7) (as a result of desiccation or cryogenic processes) filled with the material of Bk horizon (layer 6).

Thus that the BR paleosol is polygenetic, both humus accumulation process and eluvial-illuvial distribution of carbonates taking part in its development. Many authors (Antoine et al., 2009b; Terhorst et al., 2015; Meyer-Heintze et al., 2018; Adameková et al., 2021; a.o.) noted the presence of calcareous pedofeatures in paleosols dated to MIS 3. On the East Europen section south of the Likhvin section, the Bryansk soils were represented by Cambisols, giving place to Gleysols in lowered areas (Sycheva et al., 2019; 2020). Further south, near the Sea of Azov, the BR is represented by Luvic Calcisols (Panin et al., 2018). On the contrary, to the north, its profile becomes gleyed to a greater degree and reveals well pronounced cryogenic deformations (Rusakov et al., 2019). Earlier Morozova (Velichko, 2002) interpreted those soils as cryogenic-gleyed soil. As it has been found in our case (the Likhvin sequence), the BR first developed following the Cambisol type. Further on, as the climate became colder, the soil profile stayed frozen longer, and the atmospheric precipitations (and meltwater) stayed longer in the superficial horizons. The cryogenic processes gained in intensity, which promoted gleying process in the BR and development of Gleysols, probably transformed into Cryosols as the temperature continued falling.

4.1.2. The Krutitsa interstadial paleosol (MZKR)

The MZKR (layer 8) soil formation took place under rather severe climate of the interstadial. As follows from the reconstructions by Morozova and Velichko (2009), at the time of the MZKR development, the January temperature was –7 °C, that of July – +15 °C, and the mean annual temperature –0.5 °C. In the authors' opinion, the chernozem-like dark-colored soils developed under meadow and steppes or open forests of larch in the intermountain basins of the Central Altay Mountains may be considered as the present-day analogues of the MZKR (Morozova and Velichko, 2009; Velichko and Morozova, 2015). As follows from the studies of section Likhvin-1/18, the principal soil-forming process in the MZKR was a humus-accumulative one, which is in reasonable agreement with previous studies of that section (Morozova, 1981). High values of LOI 550° in the bulk samples from that paleosol confirm the presence of organic matter (Fig. 2). There was recorded charcoal remains in the MZKR microstructure found not only in A horizon (layer 8) (Fig. 9a) but also in the cryogenic wedge (Fig. 9b), penetrating from A horizon (layer 8) downwards (Fig. 3; Table 2S). No charcoal is found in the underlying MZSAL (layers 9–12) (Fig. 3). It seems probable that fires were typical of the interstadial interval. The high values of MS (Fig. 2) also suggest high mineralization of the paleosol. Fire increases the soil's temperature and stimulates biological activity (Hulbert, 1988; Ojima et al., 1994; Brye, 2006), which accounts for the presence of infillings of biogenic origin (Fig. 9c). The MZKR profile shows a concentration of clay fraction (Fig. 2), Mn and Fe-Mn nodules (Fig. 3), which suggest the soil formation under the condition of increased humidity. In the underlying horizon E (of the MZSAL layer 9), both clay-size fraction and Mn and Fe-Mn content decrease sharply. Cryoturbations (Fig. 9d, Fig. 9e) and ooid aggregates are visible in the microstructure (Fig. 9f). It seems possible that E horizon (layer 9) of the MZSAL was frozen at the time of the interstadial so that the clay fraction did not penetrate the underlying paleosol. In case of an impermeable bed formed by the frozen ground, it would cause stagnation of groundwater and enhanced anaerobic processes; the MZKR profile, however, does not show a bluish color (unlike the BR profile), and the gleying processes are indistinct. It is possible that the number of rainfalls coming to the MZKR surface was insufficient for permafrost melting in summer. According to the reconstructions, the reconstructed mean annual precipitation during the interstadial was

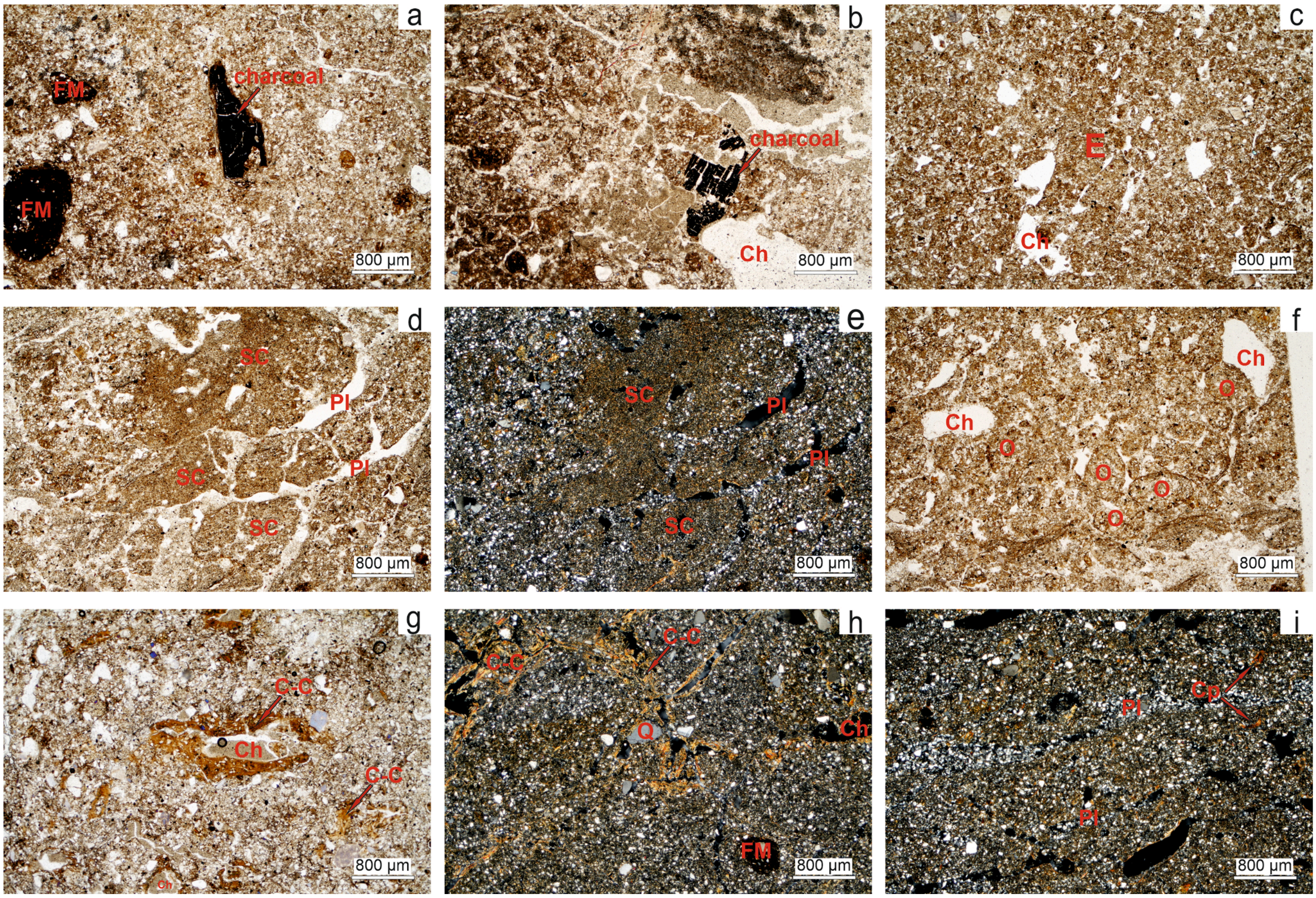

Fig. 9. Microstructure of the Mezin soil complex: a (PPL), c (PPL) - the horizon A of the MZKR; b (PPL) – wedge of the MZKR; d (PPL), e (XPL), f (PPL) - the horizon E of the MZSAL; g (PPL) - wedge of the MZSAL; h (XPL) - the horizon Btg of the MZSAL; i - (XPL) - the horizon E of the MZSAL. Legend: Ch - channels, Pl — planes, FM – Fe-Mn nodule; C-C - clayey coating; Cp – papule; Q – quartz; E – infilling; SC - silty clay; O – ooids.

220–450 mm (Morozova and Velichko, 2009). Under those conditions, the soil-forming processes were confined to A horizon (layer 8) – the only one to be heated by solar radiation in summer. The MZKR may be assigned to Folic Cambisols. The modern analogues of the soil may be found in the prairie (see Mason and Jacobs, 2017) subject to frequent fires (Collins et al., 1998).

4.1.3. The Salyn interglacial paleosol (MZSAL)

The Mikulino interglacial corresponds to MIS 5e (Eemian, last interglacial, 128–114 ka). That period was marked by the MZSAL paleosol formation on the East European Plain. The MZSAL described in section Likhvin-1/18 is noted for a texture-differentiated profile with a well pronounced eluvial E horizon (layer 9); it is classified as a Retisols. At MIS 5e interval, this type of soil formed an extensive zone (Morozova, 1995; Morozova et al., 1998; Velichko, 2002; Morozova and Velichko, 2009; Panin et al., 2019a) its genesis being discussed in many works (Morozova, 1981; Velichko et al., 2006a; Panin, 2007; Chizhikova et al., 2007; Fedorowicz et al., 2013; Jary and Ciszek, 2013; Agadjanian and Glushankova, 2017; Sycheva et al., 2017; a.o.). The high-resolution analysis applied to the section under study permitted to trace changes in the interglacial paleosol structure. Two cryogenic wedges are penetrating the MZSAL, one of them coming from E horizon (layer 9) and another from A horizon (layer 8) of the MZKR (Fig. 4-3a). The microstructure of the first wedge includes large-size illuviation coatings (Fig. 9g), their quantity (Table 2S) and texture are comparable with Btg horizon (layer 10) of the MZSAL (Fig. 9h). Outside the wedge, in the main part of E horizon (layer 9), the coatings are found as clay papulae (Fig. 9i), broken by the cryogenic processes. The wedge development mechanism could probably be similar to that described by Harris et al. (2005). The wedge attributable to the MZSAL was formed in the MIS 5d cold period when soil-forming processes faded out. At the warming (MIS 5c) the wedge was filled with material from the superficial horizons of the MZSAL. In our case, the infilling material was taken from E horizon (layer 9), as the A horizon of the MZSAL had been eroded in the intervals MIS 5e/5d or MIS 5d; there was no loess material typical of the cold stages. MIS 5c interval was marked by paleosol development, not unlike the MZKR in its structure (Little et al., 2002; Velichko and Morozova, 2015). Soil formation processes resumed their activities and exerted a noticeable influence on the material within the wedge. Inside Btg horizon (layer 10) of the MZSAL the clay matter was moved mainly by the lateral translocation (Kühn et al., 2018). That accounts for clay penetration inside the wedge and the development of the coatings similar to those in Btg horizon (layer 10) (Fig. 9h). The assumptions are confirmed by the maximum concentration of clay coatings in the middle part of the Btg horizon (layer 10) (Fig. 3) and by an increase in the clay fraction at this level (Fig. 2). The earlier formed coatings (at the time of the MZSAL development) were partly moved towards the middle part of Btg horizon (layer 10).

At the cold period MIS 5b, the cryogenic processes affected E horizon (layer 9) and partly Btg horizon (layer 10) of the MZSAL. The microstructure of those levels displays cryogenic deformations of the intra-ped mass noticeable as breaks of coatings and voids and as the presence of ooidal aggregates. A high proportion of the clay fraction (Fig. 2) is also related to permafrost. The mentioned changes are absent from or poorly pronounced in the middle or lower part of the Btg horizon (layer 10). The wedge has penetrated these horizons. Then, during the warm stage

(MIS 5a), this wedge was filled with the material of the surficial humus paleosol (generated during MIS 5c stage (Fig. 3S)). Further on, at stage MIS 5a, the paleosol was formed. The remaining soil profile of the MIS 5c being dragged into paleosol the MIS 5a, together with the above described frozen horizons of the MZSAL.

As seen from the above, the MZSAL exposed in section Likhvin-1/18 has passed through freezing and thawing stages. Formed as Retisol in the Mikulino Interglacial, it passed into Cryosol due to cryogenic processes during the MIS 5e/5d interval. At the subsequent stages (MIS 5c, 5b, 5a), it may be considered as parent rock for the interstadial paleosol profiles. However, it should be taken into account that the soil-forming processes, which resumed their activities in the MZSAL profile during the interstadials, do not reflect the dominant climate characteristics.

Under the MZSAL paleosol, Bolikhovskaya et al. (1976) distinguished a paleosol PP3. According to her data, this paleosol can be diagnosed as podzolic soil with signs of boggy soil and gleying. In the Likhvin-1/18 section, the level of PP3 paleosol may correspond to layers 11–13. According to our research, there are no well-pronounced signs of pedogenesis at this level. There are no pronounced peaks of MS, LOI 550°, and TOC (Fig. 2). In the microstructure, there are practically no clayey coatings (Fig. 3), which are characteristic of podzolic soils (Bronnikova et al., 2000). Earlier, Velichko (Little et al., 2002) also did not distinguish the level of pedogenesis under the MZSAL. It is possible that the PP3 paleosol in the section is exposed in fragments (Fig. 2S) and, therefore, we do not observe it in the Likhvin-1/18 section.

In section Likhvin-1/18 the Late Pleistocene paleosols are overlain with a thick loess horizon C (layers 4) devoid of any levels of soil formation. However, the presence of poorly developed paleosol in the layer was mentioned by Little et al. (2002). As seen in Fig. 2, the granulometry changes abruptly at 2.7 m depth: the proportion of sand increases to 31.13%, while silt proportion drops to 64.33%, the latter suggests a short-term interruption in the silt deposition.

4.1.4. The Kamenka soil complex and the Romny paleosol (ROM)

The Middle Pleistocene EKAM (layers 5–8) described in section Likhvin-2/18 presents a thick brown profile. Its microstructure abounds in clay coatings (Fig. 10a, Fig. 10b), and the high MS values suggest an active reprocessing of the paleosol by soil processes (Fig. 2). It was noted earlier (Morozova and Velichko, 2009) that the Kamenka Interglacial (MIS 7) soils mainly were Luvisols with Cambisol participation. Here the EKAM paleosols are similar to those described in the sections of Gololobovo, Strelitsa, and Ozherelye (Panin, 2007; Chizhikova et al., 2007; Panin et al., 2019a). The uppermost EKAM horizons (including eluvial ones) in the section Likhvin-2/18 had been eroded. However, the greyish-whitish horizon with a brownish hue was mentioned in the paper by Bolikhovskaya et al. (1976). As may be seen in the clay fraction distribution in coatings (Fig. 2), its proportion in the upper horizons is much more significant in comparison with Bt horizon (layer 6), which is not characteristic of the modern soils. The clay fraction transported from the overlying Ag horizon (layer 4) is accumulated at a level of ABg horizon (layer 5). A similar process had been described earlier about E horizon (layer 9) of the MZSAL. Quite possibly, the uppermost layer of the EKAM had been eroded at the transition to the cold stage MIS 6, and the paleosol lost its differentiation into horizons. That process was considered in details about Luvisols in Poland (Świtoniak et al., 2016). The information available at present permits the EKAM in section Likhvin-2/18 to be compared with Luvisols' modern analogues (Cutanic), found at present in Latvia, Poland, and Hungary (Świtoniak and Charzyński, 2014).

The soil-forming level described above the EKAM soil and attributed to the ROM by Velichko (Little et al., 2002) has poorly pronounced characteristics of a well-developed soil. The paleosol profile is heavily gleyed and consists of Ag horizon (layer 4) only; the layer is cryoturbated, some charcoal remains, and coatings are noticeable in microstructure (Fig. 10c, Fig. 10d). Earlier, we described those specific features in the Mezin soil complex, section Likhvin-1/18. As seen in Fig. 2, the graphs of the distribution of the clay fraction, LOI 550° and 950° of the paleosols of the Mezin soil complex, and the ROM and EKAM are practically similar. So it is possible that ROM may be LKAM, in fact, and therefore the section Likhvin-2/18 presents the Kamenka soil complex. The paleosol of layer 4 in section Likhvin-2/18 may be classified with Gleysols.

According to Bolikhovskaya et al. (1976), four paleosols under the Dnieper till are located in the Likhvin section. Velichko (Little et al., 2002) distinguished three levels of soil formation in the section. In our case, we can speak only about two paleosols, which they also described. In the Likhvin-2/18 section, we did not find the Likhvin interglacial paleosol (MIS 9), which had an eluvial horizon (Moskvitin, 1967) that could be attributed to Retisols.

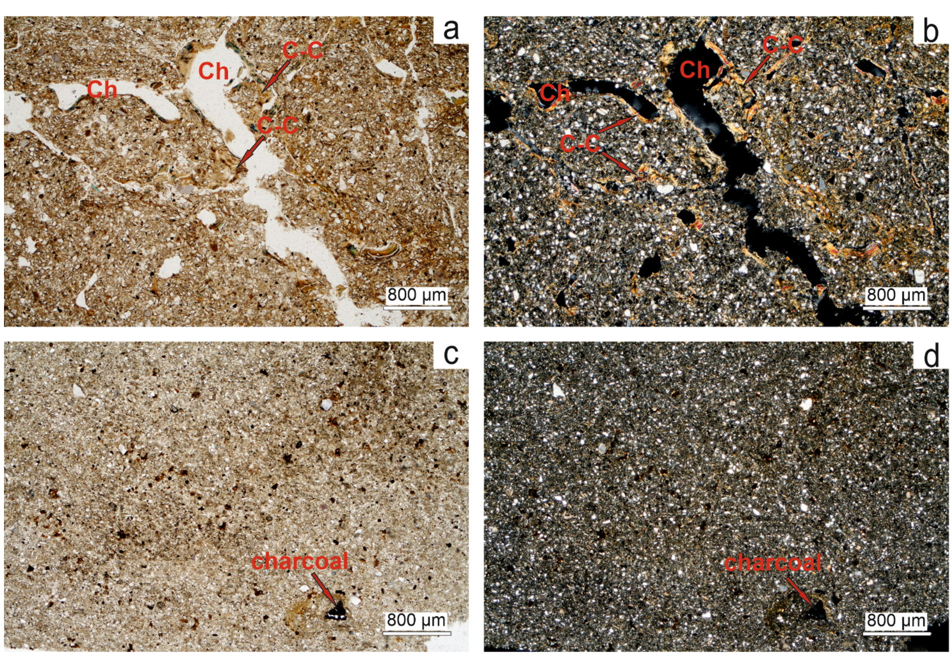

Fig. 10. Microstructure of the EKAM and the ROM: a (PPL), b (XPL) - the horizon Bt of the EKAM; c (PPL), d (XPL) – ROM.Legend: Ch - channels, C-C - clayey coating.

4.2. OSL and AMC dates in the Likhvin section stratigraphy

The stratigraphic position of BR in the Likhvin sequence is considered in details by Little et al. (2002), the authors having dated it to MIS 3 (Fig 11). AMS date of 29987 cal BP corresponds to this interval. OSL date of 67 ± 7 ka in the Bk horizon (layer 6) of this paleosol does not contradict these conclusions. The OSL analysis determines the age of the soil-forming rock accumulated during the MIS 4, and the soil formation took place in a later period. This sequence is typical for modern soil, where the main processes of soil formation took place in the Holocene (MIS 1), and the loess material of MIS 2 serves as the basis for the soil. It is confirmed by 17.9 ± 1.1 ka and 27.7 ± 1.9 ka dates in the loess horizon C (layer 4) (Fig. 11).

As to the MZKR, the authors mentioned above (Little et al., 2002) attributed it to MIS 5c, but our results argue for the paleosol being correlated with MIS 5a. OSL dates of 88 ± 6 ka and 86 ± 6 ka in horizon A (layer 8) correlate with MIS 5b, which correspond to the cold stage of accumulation of loess material. During the warming period of MIS 5a, an interstadial type of paleosol is formed on this substrate, the so-called MZKR paleosol. The overlying deposits of layers 7 and 6 formed in MIS 4 do not allow layer 8 to be attributed to the MIS 3 interval. In horizon E (layer 9), the date is 86 ± 6 ka, corresponding to the MIS interval 5b. This age inversion can only be explained by the movement of material from layer 8 to layer 9 caused by cryogenic processes. Simultaneously, between layers 8 and 9, the MIS 5c paleosol, which Velichko et al. (2011) called the MZKR paleosol, should be stratigraphically expressed. It is possible that erosion processes demolished the MZKR paleosol in the transition interval from MIS 5c to 5d. Therefore, in the Likhvin-1/18 section, we observe the paleosol profile formed in MIS 5a, but we understand that this statement needs to be confirmed by additional studies.

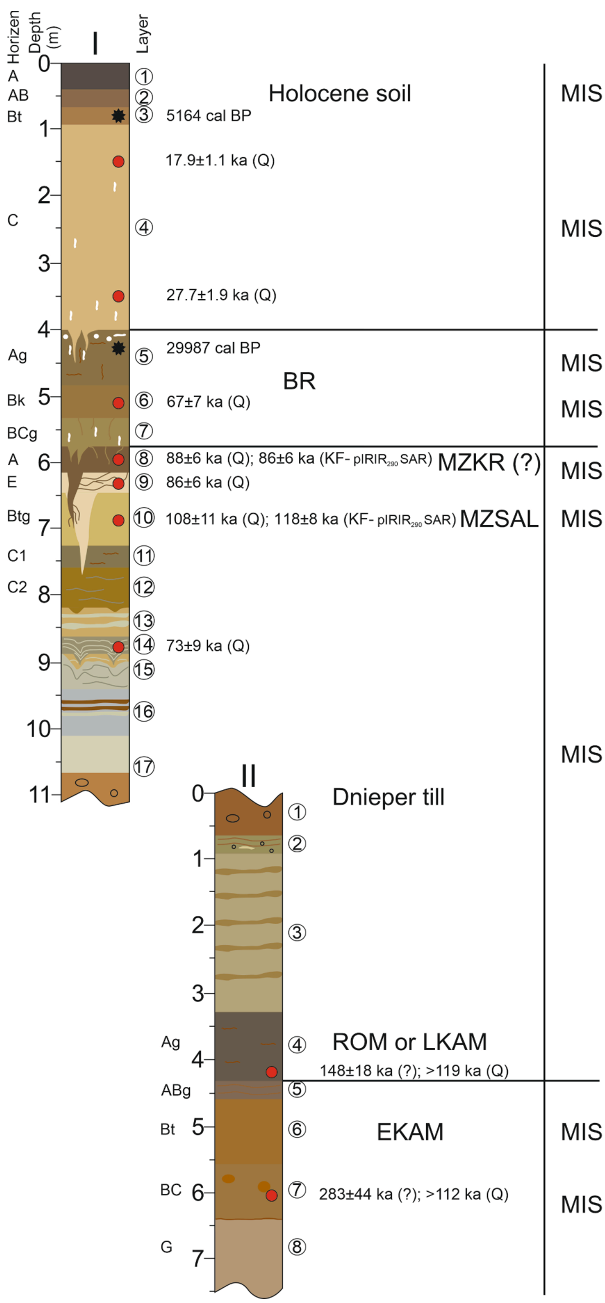

Fig. 11. Stratigraphy of Likhvin-1/18 (I) and Likhvin-2/18 (II) sections. See legend in Tables 1S and 3S. See Fig. 2 for the legend for the section column. Q - quartz and KF - K-rich feldspar.

In the MZSAL paleosol, two dates were obtained in the middle part of the Btg horizon (layer 10), which partially correspond to the interval 128–114 ka of MIS 5e (Fig. 11). The date of 108 ± 11 ka by quartz within the error range can refer to MIS 5e and MIS 5d, and the date 118 ± 8 ka by feldspar refers only to MIS 5e. In the chronostratigraphic scheme by Velichko et al. (2011), the MZSAL paleosol correlates with MIS 5e. The paleosol profile is well developed; there is a textural differentiation into the soil horizons E and Btg, which can be traced at the micro-level (Fig. 3) and according to the physico-chemical analyses data (Fig. 2). All these soil features are characteristic of interglacial paleosols (Panin et al., 2019a; Sycheva et al., 2020), where soil formation processes took place for a long time. Therefore, it can be stated with great confidence that the MZSAL paleosol in the Likhvin-1/18 section was formed during the interglacial period MIS 5e. We believe that the obtained stratigraphy needs to be confirmed by a more careful selection of possible dates. Since in layer 14 of the Likhvin-1/18 section, the accepted date of 73 ± 9 ka does not correspond to this section’s stratigraphy.

The ROM and LKAM paleosols were formed in the interstadial period of MIS 6 (Velichko and Morozova, 2015). In the Likhvin-2/18 section, the date 148 ± 18 ka in layer 4 corresponds to this interval (Fig. 11). But the absence of additional OSL samples in this layer does not allow us to specify the age of the Ag paleosol horizon and relate it to the ROM and LKAM paleosols. The OSL date of 283 ± 44 ka in the soil-forming horizon BC (layer 7) of the EKAM paleosol correlates with MIS 8. The Bt (layer 6) and ABg (layer 5) horizons were formed later than this date, so it can be assumed that the main soil-formation processes in the EKAM paleosol also took place later. Given that the EKAM paleosol is interglacial and in the upper layer 4 is limited by the obtained age of MIS 6, this paleosol can be attributed to MIS 7. Unfortunately, we are not sure of the reliability of the dates given here, and the obtained infinite ages (>119 ka; >112 ka) do not correspond to the studied time interval. Further investigations should focus on the age refinement of subtill deposits in the Likhvin-2/18 section by OSL dating of K-rich feldspar.

5. Conclusions

Only five paleosols have been found in the Likhvin section in the course of our investigations. The high-resolution analyses gave us an insight into the structure of the paleosols studied in the LPS of the section and permitted us to compare them with the modern soils. Based on the study of climatic conditions, under which the modern analogues of paleosols develop (Kottek et al., 2006; Shoba, 2011), we could reconstruct the climate dominant in the region in the Late and Middle Pleistocene (Table 1).

The BR, MZSAL, and EKAM paleosols identified in sections Likhvin-1/18 and Likhvin-2/18 are quite common on the East European Plain and fit well the chronostratigraphic scheme.

The MZKR in the Likhvin-1/18 section, according to the results of OSL analysis, corresponds to MIS 5a; it was previously believed that this

Table 1
The climate conditions reconstruction of the paleosol development periods during Late and Middle Pleistocene.

MIS	Paleosol	Modern soil analogues	Köppen – Geiger Climate Classification
1	Modern soil	Phaeozems	Dfb
3	BR	Cryosols	ET
3	BR	Gleysols	Dfc, Dfd
3	BR	Cambisols	Dfb
5a	so-called the MZKR	Folic Cambisols	Dfd
5c	MZKR	eroded (?)	
5e-5d	MZSAL	Cryosols	ET
5e	MZSAL	Retisols	Dfc
6	ROM or LKAM	Gleysols	Dfc, Dfd
7	EKAM	Luvisols (Cutanic)	Cfb, Dfb

paleosol developed in the MIS 5c interval. This assumption requires additional research.

The ROM on the East European Plain is not sufficiently studied, so we have not enough information to assert layer 4 in the Likhvin-2/18 section as belonging to this paleosol. Perhaps the ROM is the LKAM of the Kamenka soil complex, and this conclusion needs further research. The OSL dates obtained during our study in the Likhvin-2/18 section require further refinement and confirmation by other OSL dates.

Declaration of Competing Interest

The authors declare that they have no known competing financial interests or personal relationships that could have appeared to influence the work reported in this paper.

Acknowledgements

The reported study was funded by the Institute of Geography of the Russian Academy of Sciences State Task № 0148-2019-0005 (manuscript preparation) and by RFBR and NSFC according to the research projects № 20-55-53003, RFBR and DST № 19-54-45008 (OSL dating of two samples), and according to State Task № 0191-2019-0048 (measurements of the organic carbon content). The authors acknowledge the help of I.I. Spasskaya in language editing. We thank E.A. Konstantinov and his group for assistance in the laboratory and are grateful to E.P. Zazovskaya for preparing the samples for AMS analysis. We are also grateful to G.R. Glazman for measuring the color of the samples, and A.L. Zakharov for topographic and geodetic profiling of the Likhvin section, and I.V. Timofeeva for assistance in OSL dating. We are grateful to anonymous reviewers for the constructive comments and valuable suggestions that significantly improved the initial paper.

Appendix A. Supplementary data

Supplementary data to this article can be found online at https://doi.org/10.1016/j.catena.2021.105445.

References

Adameková, K., Lisá, L., Neruda, P., Petřík, J., Doláková, N., Novák, J., Volánek, J., 2021. Pedosedimentary record of MIS 5 as an interplay of climatic trends and local conditions: Multi-proxy evidence from the Palaeolithic site of Moravský Krumlov IV (Moravia, Czech Republic). Catena 105174. https://doi.org/10.1016/j.catena.2021.105174.

Agadjanian, A.K., 1977. Quartäre Kleinsäuger aus der Russischen Ebene. Quartär 27–28 (28), 111–145.

Agadjanian, A.K., Glushankova, N.I., 2017. Quaternary stratigraphy and developmental history of the central Russian periglacial–loessal province. Stratigr. Geol. Correl. 25 (4), 445–462. https://doi.org/10.1134/S0869593817040025.

Alisov, B.P., 1947. Climatic regions and regions of the USSR. Lomonosov Moscow State University, Research Institute of Geography, Moscow, Geografgiz (in Russian).

Antoine, P., Rousseau, D.-D., Fuchs, M., Hatté, C., Gauthier, C., Marković, S.B., Jovanović, M., Gaudenyi, T., Moine, O., Rossignol, J., 2009a. High-resolution record of the last climatic cycle in the southern Carpathian Basin (Surduk, Vojvodina, Serbia). Quat. Int. 198 (1–2), 19–36. https://doi.org/10.1016/j.quaint.2008.12.008.

Antoine, P., Rousseau, D.-D., Moine, O., Kunesch, S., Hatté, C., Lang, A., Tissoux, H., Zöller, L., 2009b. Rapid and cyclic aeolian deposition during the Last Glacial in European loess: a high-resolution record from Nussloch. Germany. Quat. Sci. Rev. 28 (25–26), 2955–2973. https://doi.org/10.1016/j.quascirev.2009.08.001.

Arinushkina, E.V., 1970. Guide on the Chemical Analysis of Soils. Moscow State University Publishing House, Moscow (in Russian).

Blott, S.J., Pye, K., 2001. GRADISTAT: A grain size distribution and statistics package for the analysis of unconsolidated sediments. Earth Surf. Proc. Land. 26, 1237–1248.

Bogolubov, N.N., 1904. The vicinity of Likhvin. In: Bogolubov, N.N., (Ed.), Geological materials of Kaluga province. In parts 2, Kaluga, Printing House of the Provincial Zemsky Council, pp. 290-337. (in Russian).

Bolikhovskaya, N.S., Sudakova, N.G., 1996. The Chekalin (Likhvin) reference section in the Russian plain and its significance for pleistocene stratigraphy and correlation. Stratigr. Geol. Correl. 4 (3), 294–304.

Bolikhovskaya, N.S., Molodkov, A.N., 2006. East European loess–palaeosol sequences: Palynology, stratigraphy and correlation. Quat. Int. 149 (1), 24–36. https://doi.org/10.1016/j.quaint.2005.11.015.

Bolikhovskaya, N.S., Glushankova, N.I., Rengarten, N.V., Sudakova, N.G., 1976. Buried soil of the Likhvin (Chekalin) section. Bulletin of the Commission for Study of the Quaternary, 45. Moscow, Nauka, pp. 30–44. (in Russian).

Bronnikova, M.A., Sedov, S.N., Targulian, V.O., 2000. Clay, iron-clay, and humus-clay coatings in the eluvial part of soddy-podzolic soils profile. Eurasian Soil Sci. 33 (6), 577–584.

Brye, K.R., 2006. Soil physiochemical changes following 12 years of annual burning in a humid-subtropical tallgrass prairie: a hypothesis. Acta Oecologica 30 (3), 407–413. https://doi.org/10.1016/j.actao.2006.06.001.

Bulygina, O.N, Razuvaev, V.N., Korshunova, N.N., Shvets, N.V., 2015. Description of the dataset the monthly precipitation totals, air temperature and vapor pressure in the air at the meteorological stations of Russia. The certificate of state registration database № 2015620394 (in Russian). http://meteo.ru/data.

Buylaert, J.P., Vandenberghe, D., Murray, A.S., Huot, S., De Corte, F., Van den Haute, P., 2007. Luminescence dating of old (>70 ka) Chinese loess: A comparison of single-aliquot OSL and IRSL techniques. Quat. Geochronology 2 (1–4), 9–14. https://doi.org/10.1016/j.quageo.2006.05.028.

Chizhikova, N.P., Morozova, T.D., Panin, P.G., 2007. Mineralogical composition of the clay fraction and micromorphology of the Middle and Late Pleistocene paleosols and loesses of the center part of the East European plain. Eurasian Soil Sci. 40 (12), 1343–1354. https://doi.org/10.1134/S1064229307120125.

Collins, S.L., Knapp, A.K., Briggs, J.M., Blair, J.M., Steinauer, E.M., 1998. Modulation of diversity by grazing and mowing in native tallgrass prairie. Science 280 (5364), 745–747. https://doi.org/10.1126/science.280.5364.745.

Derbyshire, E., Owen, L.A., 2018. Glacioaeolian processes, sediments, and landforms. In: Menzies, J., van der Meer, J.J.M., (Eds.), Past Glacial Environments, Elsevier, pp. 273-308. https://doi.org/10.1016/B978-0-08-100524-8.00008-7.

Dobrodeyev, O.P., Il'ichev, V.A., 1974. Age of loess and fossil soils of the Russian Plain and their correlation with glacial events of the Pleistocene. Transactions (Doklady) of the Russian Academy of Science. Earth Science Section 214, 54–56.

Duller, G.A.T., 2003. Distinguishing quartz and feldspar in single grain luminescence measurements. Radiat. Meas. 37 (2), 161–165. https://doi.org/10.1016/S1350-4487(02)00170-1.

Duller, G.A.T., 2015. The Analyst software package for luminescence data: overview and recent improvements. Ancient TL 33 (1), 35–42.

Durand, N., Monger, H.C., Canti, M.G., Verrecchia, E.P., 2018. Chapter 9 - Calcium carbonate features. In: Stoops, G., Marcelino, V., Mees, F. (Eds.), Interpretation of Micromorphological Features of Soils and Regoliths (Second Edition). Elsevier, Amsterdam, pp. 205–258. https://doi.org/10.1016/B978-0-444-63522-8.00009-7.

FAO, 2006. Guidelines for Soil Description. fourth ed. Rome.

FAO–ISRIC, 1990. Guidelines for profile description. 3rd Edition. Rome.

Faustov, S.S., Il'ichev, V.A., Bol'shakov, V.A., 1974. Paleomagetic and thermoluminescence analyses of the Likhvin section. Doklady Earth Sci. Sections 214 (1–6), 123–125.

Fedorowicz, S., Lanczont, M., Bogucki, A., Kusiak, J., Mroczek, P., Adamiec, G., Bluszcz, A., Moska, P., Tracz, M., 2013. Loess-paleosol sequence at Korshiv (Ukraine): Chronology based on complementary and parallel dating (TL, OSL), and litho-pedosedimentary analyses. Quat. Int. 296, 117–130. https://doi.org/10.1016/j.quaint.2012.06.001.

Fitzsimons, S., Lorrain, R., 2011. Subglacial Processes. In: Singh, V.P., Singh, P., Haritashya, U.K. (Eds.), Encyclopedia of snow, ice and glaciers. Encyclopedia of earth sciences series. Springer, Dordrecht. https://doi.org/10.1007/978-90-481-2642-2.

Fitzsimons, S., Howarth, J., 2018. Glaciolacustrine processes. In: Menzies, J., van der Meer, J.J.M., (Eds.), Past Glacial Environments, Elsevier, pp. 309-334, https://doi.org/10.1016/B978-0-08-100524-8.00009-9.

Glushankova, N.I., 1971. Some characteristics of the group composition of the humus of the buried soils of the Likhvin key section. Bulletin of Moscow University, № 5, Geography, 109-113. (in Russian).

Grichuk, V.P., 1950. Vegetation of the Russian Plain in the Lower and Middle Quaternary. In: Gerasimov, I.I., (Ed.), Materials on geomorphology and paleogeography of the USSR, Proceedings of the IG of the USSR Academy of Sciences, 46(3). pp. 5-202. (in Russian).

Haase, D., Fink, J., Haase, G., Ruske, R., Pécsi, M., Richter, H., Altermann, M., Jäger, K.-D., 2007. Loess in Europe - its spatial distribution based on a European Loess Map,

scale 1:2,500,000. Quat. Sci. Rev. 26 (9–10), 1301–1312. https://doi.org/10.1016/j.quascirev.2007.02.003.
Hansen, V., Murray, A., Buylaert, J.-P., Yeo, E.-Y., Thomsen, K., 2015. A new irradiated quartz for beta source calibration. Radiat. Meas. 81, 123–127. https://doi.org/10.1016/j.radmeas.2015.02.017.
Harris, C., Murton, J.B., Davies, M.C.R., 2005. An analysis of mechanisms of ice-wedge casting based on geotechnical centrifuge simulations. Geomorphology 71 (3–4), 328–343. https://doi.org/10.1016/j.geomorph.2005.03.006.
Heiri, O., Lotter, A.F., Lemcke, G., 2001. Loss on ignition as a method for estimating organic and carbonate content in sediments: reproducibility and comparability of results. J. Paleolimnol. 25, 101–110. https://doi.org/10.1023/A:1008119611481.
Hou, K., Qian, H., Zhang, Y., Zhang, Q., 2020. Influence of tectonic uplift of the Qinling Mountains on the paleoclimatic environment of surrounding areas: Insights from loess–paleosol sequences, Weihe Basin, central China. Catena 187, 104336. https://doi.org/10.1016/j.catena.2019.104336.
Hulbert, L.C., 1988. Causes of fire effects in tallgrass prairie. Ecology 69 (1), 46–58.
Huntley, D.J., Baril, M.R., 1997. The K content of the K-feldspars being measured in optical dating or in thermoluminescence dating. Ancient TL 15, 11–13.
Huntley, D.J., Hancock, R.G.V., 2001. The Rb contents of the K-feldspar grains being measured in optical dating. Ancient TL 19, 43–46.
IUSS Working Group WRB. 2015. World Reference Base for Soil Resources 2014, update 2015 International soil classification system for naming soils and creating legends for soil maps. World Soil Resources Reports No. 106. FAO, Rome.
Jary, Z., Ciszek, D., 2013. Late Pleistocene loess-palaeosol sequences in Poland and western Ukraine. Quat. Int. 296, 37–50. https://doi.org/10.1016/j.quaint.2012.07.009.
Jain, M., Murray, A.S., Bøtter-Jensen, L., 2003. Characterisation of blue-light stimulated luminescence components in different quartz samples: implications for dose measurement. Radiat. Meas. 37 (4–5), 441–449. https://doi.org/10.1016/S1350-4487(03)00052-0.
Karpukhin, S.S., Lavrov, A.S., 1974. Direction of movement and position of the contact zone of the Dnieper ice sheets on the Russian Plain. Dokl. Academy of Sciences of the USSR. 216 (1), 158–161 (in Russian).
Krauß, L., Zens, J., Zeeden, C., Schulte, P., Eckmeier, E., Lehmkuhl, F., 2016. A multi-proxy analysis of two loess-paleosol sequences in the Northern Harz Foreland, Germany. Palaeogeogr. Palaeoclimatol. Palaeoecol. 461, 401–417. https://doi.org/10.1016/j.palaeo.2016.09.001.
Kühn, P., Aguilar, J., Miedema, R., Bronnikova, M., 2018. Chapter 14 - Textural pedofeatures and related horizons. In: Stoops, G., Marcelino, V., Mees, F. (Eds.), Interpretation of Micromorphological Features of Soils and Regoliths (Second Edition). Elsevier, Amsterdam, pp. 377–423. https://doi.org/10.1016/B978-0-444-63522-8.00014-0.
Kottek, M., Grieser, J., Beck, C., Rudolf, B., Rubel, F., 2006. World Map of the Köppen-Geiger climate classification updated. Meteorol. Z. 15, 259–263. https://doi.org/10.1127/0941-2948/2006/0130.
Lai, Z.P., 2010. Chronology and the upper dating limit for loess samples from Luochuan section in the Chinese Loess Plateau using quartz OSL SAR protocol. Journal of Asian Earth Sci. 37 (2), 176–185. https://doi.org/10.1016/j.jseaes.2009.08.003.
Lapp, T., Kook, M., Murray, A.S., Thomsen, K.J., Buylaert, J.-P., Jain, M., 2015. A new luminescence detection and stimulation head for the Risø TL/OSL reader. Radiat. Meas. 81, 178–184. https://doi.org/10.1016/j.radmeas.2015.02.001.
Liu, C., Dupont-Nivet, G., Wang, W., Deng, C., 2021. Magnetic response to pedogenesis in aerobic soils of different weathering degree. Palaeogeogr. Palaeoclimatol. Palaeoecol. 567, 110240 https://doi.org/10.1016/j.palaeo.2021.110240.
Liritzis, I., Stamoulis, K., Papachristodoulou, C., Ioannides, K., 2013. A re-evaluation of radiation dose-rate conversion factors. Mediterranean Archaeology and Archaeometry 13 (3), 1–13.
Little, E.C., Lian, O.B., Velichko, A.A., Morozova, T.D., Nechaev, V.P., Dlussky, K.G., Rutter, N.W., 2002. Quaternary stratigraphy and optical dating of loess from the East European Plain (Russia). Quat. Sci. Rev. 21 (14–15), 1745–1762. https://doi.org/10.1016/S0277-3791(01)00151-2.
Lu, H., Jia, J., Yin, Q., Xia, D., Gao, F., Liu, H., Fan, Y., Li, Z., Wang, X., Berger, A., Oimuhammadzoda, I., Gadoev, M., 2020. Atmospheric dynamics patterns in southern Central Asia since 800 ka revealed by loess-paleosol sequences in Tajikistan. Geophys. Res. Lett. 47(17), e2020GL088320, 1–10. https://doi.org/10.1029/2020GL088320.
Markova, A.K., 2006. Likhvin Interglacial small mammal faunas of Eastern Europe. Quat. Int. 149 (1), 67–79. https://doi.org/10.1016/j.quaint.2005.11.019.
Mason, J.A., Jacobs, P.M., 2017. Soils and palaeosols in Glacial Environments. In: Menzies, J., Jaap J.M. van der Meer (Eds.), Past Glacial Environments: Second Edition, pp. 585-603. https://doi.org/10.1016/B978-0-08-100524-8.00018-X.
Mejdahl, V., 1987. Internal radioactivity in quartz and feldspar grains. Ancient TL 5, 10–17.
Meyer-Heintze, S., Sprafke, T., Schulte, P., Terhorst, B., Lomax, J., Fuchs, M., Lehmkuhl, F., Neugebauer-Maresch, C., Einwögerer, T., Händel, M., Simon, U., Solís Castillo, B., 2018. The MIS 3/2 transition in a new loess profile at Krems-Wachtberg East – a multi-methodological approach. Quat. Int. 464, 370–385. https://doi.org/10.1016/j.quaint.2017.11.048.
Morozova, T.D., 1981. Evolution of Late Pleistocene Soil Cover in Europe. Nauka Press, Moscow (in Russian).
Morozova, T.D., 1995. Identification of paleosol types and their applicability for paleoclimatic reconstructions. GeoJournal 36, 199–205. https://doi.org/10.1007/BF00813170.
Morozova, T.D., Velichko, A.A., 2009. Paleosols, Quaternary. In: Gornitz, V. (Ed.), Encyclopedia of Paleoclimatology and Ancient Environments. pp. 273-279. https://doi.org/10.1007/978-1-4020-4411-3_179.
Morozova, T.D., Velichko, A.A., Dlussky, K.G., 1998. Organic carbon content in the late pleistocene and holocene fossil soils (reconstruction for Eastern Europe). Global Planet. Change 16–17, 131–151. https://doi.org/10.1016/S0921-8181(98)00027-7.
Moska, P., Jary, Z., Adamiec, G., Bluszcz, A., 2019. High resolution dating of loess profile from Strzyżów (Horodło Plateau-Ridge, Volhynia Upland). Quat. Int. 502, 18–29. https://doi.org/10.1016/j.quaint.2018.02.016.
Moskvitin, A.I., 1931. The new data about Likhvin outcrop. Bulleten Moskovskogo Obshestva Ispytatelei Prirody, Otdelenie Geologichskoe 9 (1–2), 57–67 (in Russian).
Moskvitin, A.I., 1967. Pleistocene stratigraphy of the European Part of the USSR. Transactions, 156, Moscow, Nauka. (in Russian).
Munsell Color, 2000. Munsell Soil Color Charts. GretagMacbeth, New Windsor, NY.
Murray, A.S., Wintle, A.G., 2000. Luminescence dating of quartz using an improved single-aliquot regenerative-dose protocol. Radiat. Meas. 32 (1), 57–73. https://doi.org/10.1016/S1350-4487(99)00253-X.
Murray, A.S., Wintle, A.G., 2003. The single aliquot regenerative dose protocol: potential for improvements in reliability. Radiat. Meas. 37 (4–5), 377–381. https://doi.org/10.1016/S1350-4487(03)00053-2.
Murray, A.S., Marten, R., Johnston, A., Martin, P., 1987. Analysis for naturally occuring radionuclides at environmental concentrations by gamma spectrometry. J. Radioanal. Nucl. Chem. Art. 115, 263–288. https://doi.org/10.1007/BF02037443.
Murray, A.S., Buylaert, J.-P., Henriksen, M., Svendsen, J.-I., Mangerud, J., 2008. Testing the reliability of quartz OSL ages beyond the Eemian. Radiat. Meas. 43 (2–6), 776–780. https://doi.org/10.1016/j.radmeas.2008.01.014.
Nazarov, D.V., Nikolskaya, O.A., Gladysheva, A.S., Zhigmanovsky, I.V., Ruchkin, M.V., Merkuliev, A.V., 2020. Pleistocene marine formations of the lower Yenissei basin, Arctic Russia: OSL age, facial and paleontological characteristics. Regional Geology and Metallogeny 82, 16–34 (in Russian).
Nejman, L., Wood, R., Wright, D., Lisá, L., Nerudová, Z., Neruda, P., Přichystal, A., Svoboda, J., 2017. Hominid visitation of the Moravian Karst during the Middle-Upper Paleolithic transition: New results from Pod Hradem Cave (Czech Republic). J. Hum. Evol. 108, 131–146. https://doi.org/10.1016/j.jhevol.2017.03.015.
Ojima, D.S., Schimel, D.S., Parton, W.J., Owensby, C.E., 1994. Long- and short-term effects of fire on nitrogen cycling in tallgrass prairie. Biogeochemistry 24 (2), 67–84.
Panin, P.G., 2007. Specificity of the morphology of interglacial and interstadial paleosol complexes of the Middle and Late Pleistocene in the center of the East European Plain. Eurasian Soil Sci. 40 (2), 126–139.
Panin, P.G., Timireva, S.N., Morozova, T.D., Velichko, A.A., 2019a. Micromorphology of the Late and Middle Pleistocene paleosols of the central East European Plain. Geography, Environment, Sustainability. 12 (1), 34–62. https://doi.org/10.24057/2071-9388-2018-32.
Panin, P.G., Timireva, S.N., Morozova, T.D., Kononov, Yu.M., Velichko, A.A., 2018. Morphology and micromorphology of the loess-paleosol sequences in the south of the East European plain (MIS1–MIS17). Catena 168, 79–101. https://doi.org/10.1016/j.catena.2018.01.032.
Panin, P.G., Timireva, S.N., Konstantinov, E.A., Kalinin, P.I., Kononov, Yu.M., Alekseev, A.O., Semenov, V.V., 2019b. Plio-Pleistocene paleosols: Loess-paleosol sequence studied in the Beregovoye section, the Crimean Peninsula. Catena 172, 590–618. https://doi.org/10.1016/j.catena.2018.09.020.
Pisareva, V.V., Sudakova, N.G., Zyganova, I.S., Karpukhina, N.V., Zakharov, A.L., 2019. The disputable problems of the middle neopleocene stratigraphy of the central region of the East-European plain. Bulletin of the Commission for study of the Quaternary, 77. Moscow, GEOS, 49-85. (in Russian, English abstract, references).
Prescott, J.R., Hutton, J.T., 1994. Cosmic ray contributions to dose rates for luminescence and ESR dating: Large depths and long-term time variations. Radiat. Meas. 23 (2–3), 497–500. https://doi.org/10.1016/1350-4487(94)90086-8.
Reimer, P.J., Bard, E., Bayliss, A., Beck, J.W., Blackwell, P.G., Bronk, R.C., Buck, C.E., Cheng, H., Edwards, R.L., Friedrich, M., Grootes, P.M., Guilderson, T.P., Haflidason, H., Hajdas, I., Hatté, C., Heaton, T.J., Hoffmann, D.L., Hogg, A.G., Hughen, K.A., Kaiser, K.F., Kromer, B., Manning, S.W., Niu, M., Reimer, R.W., Richards, D.A., Scott, E.M., Southon, J.R., Staff, R.A., Turney, C.S.M., van der Plicht, J., 2013. IntCal13 and Marine13 Radiocarbon Age calibration curves 0–50,000 years cal BP. Radiocarbon 55 (4), 1869–1887. https://doi.org/10.2458/azu_js_rc.55.16947.
Retallack, G.J., 2019. Soils of the Past: An Introduction to Paleopedology. Third Edition, Wiley-Blackwell.
Rusakov, A.V., Korkka, M.A., Kerzum, P.P., Simakova, A.N., 2007. Paleosols in the moraine-mantle loam sequence of northeastern Europe: The memory of pedogenesis rates and evolution of the environment during OIS3. Catena 71 (3), 456–466. https://doi.org/10.1016/j.catena.2007.03.023.
Sedov, S., Rusakov, A., Sheinkman, V., Korkka, M., 2016. MIS3 paleosols in the center-north of Eastern Europe and Western Siberia: Reductomorphic pedogenesis conditioned by permafrost? Catena 146, 38–47. https://doi.org/10.1016/j.catena.2016.03.022.
Shoba, S.A. (Editor-in-Chief), 2011. National Soil Atlas of Russia. Moscow, Astrel. (in Russian). http://soilatlas.ru.
Stremme, H.E., 1998. Correlation of Quaternary pedostratigraphy from Western to Eastern Europe. Catena 34 (1–2), 105–112. https://doi.org/10.1016/S0341-8162(98)00084-8.
Sudakova, N.G., 1975. The new data about the Likhvin stratotype. Dokl. Akad. Nauk SSSR 221 (1), 168–171 (in Russian).
Sudakova, N.G., Aleshinskaya, Z.V., 1974. Early and Middle Pleistocene. Chapter 3. North-West and the Center of the European part of the USSR. In: Zubkova, V.A., Afanasyev, G.D., Badinova, V.P., Borovikov, L.I., Kochegura, V.V., Cherdyntsev, V.V. (Eds.), Geochronology of the USSR. Tom 3. The latest stage. (in Russian), Leningrad, "Nedra", pp. 49–55.

Sudakova, N.G., Bol'shakov, V.A., 1977. An oldest till near the town of Chekalin at the Oka. River. Dokl. Akad. Nauk SSSR 223 (6), 1176–1179 (in Russian).

Sudakova, N.G., Antonov, S.I., 2021. Regional features of the geomorphological structure of the ancient glacial region in the center of the Russian plain. Geomorphology, 1, 100-108. (in Russian). https://doi.org/10.31857/S0435428121010120.

Stuiver, M., Reimer, P.J., 1993. Extended 14C data base and revised CALIB 3.0 14C age calibration program. Radiocarbon 35, 215–230. https://doi.org/10.1017/S0033822200013904.

Stoops, G., 2003. Guidelines for Analysis and Description of Soil and Regolith Thin Sections. Soil Science Society of America, Madison, Wisconsin.

Stoops, G., Marcelino, V., Mees, F. (Eds.), 2010. Interpretation of Micromorphological Features of Soils and Regoliths. Elsevier, Amsterdam.

Sycheva, S., Khokhlova, O., Pushkina, P., Ukrainsky, P., 2019. Interrelations of the Bryansk paleosol (end of MIS 3) with the Holocene surface soils in micro-depressions of the central forest-steppe within the Russian Upland. Catena 172, 619–633. https://doi.org/10.1016/j.catena.2018.09.021.

Sycheva, S., Frechen, M., Terhorst, B., Sedov, S., Khokhlova, O., 2020. Pedostratigraphy and chronology of the Late Pleistocene for the extra glacial area in the Central Russian Upland (reference section Aleksandrov quarry). Catena 194, 104689. https://doi.org/10.1016/j.catena.2020.104689.

Sycheva, S.A., Sedov, S.N., Bronnikova, M.A., Targulian, V.O., Solleiro-Rebolledo, E., 2017. Genesis, evolution, and catastrophic burying of the Ryshkovo paleosol of the Mikulino interglacial (MIS 5e). Eurasian Soil Sci. 50 (9), 991–1009. https://doi.org/10.1134/S1064229317090071.

Świtoniak, M., Charzyński, P., 2014. Soil sequences atlas. Nicolaus Copernicus University Press.

Świtoniak, M., Mroczek, P., Bednarek, R., 2016. Luvisols or Cambisols? Micromorphological study of soil truncation in young morainic landscapes - Case study: Brodnica and Chełmno Lake Districts (North Poland). Catena 137, 583–595. https://doi.org/10.1016/j.catena.2014.09.005.

Tecsa, V., Mason, J.A., Johnson, W.C., Miao, X., Constantin, D., Radu, S., Magdas, D.A., Veres, D., Marković, S.B., Timar-Gabor, A., 2020. Latest Pleistocene to Holocene loess in the central Great Plains: Optically stimulated luminescence dating and multi-proxy analysis of the enders loess section (Nebraska, USA). Quat. Sci. Rev. 229, 106130 https://doi.org/10.1016/j.quascirev.2019.106130.

Terhorst, B., Sedov, S., Sprafke, T., Peticzka, R., Meyer-Heintze, S., Kühn, P., Solleiro Rebolledo, E., 2015. Austrian MIS 3/2 loess-palaeosol records-Key sites along a west-east transect. Palaeogeogr. Palaeoclimatol. Palaeoecol. 418, 43–56. https://doi.org/10.1016/j.palaeo.2014.10.020.

Timireva, S.N., Velichko, A.A., 2006. Depositional environments of the Pleistocene loess-soil series inferred from sand grain morphoscopy — a case study of the East European Plain. Quat. Int. 152–153, 136–145. https://doi.org/10.1016/j.quaint.2005.12.013.

Timar-Gabor, A., Vandenberghe, D.A.G., Vasiliniuc, S., Panaoitu, C.E., Panaiotu, C.G., Dimofte, D., Cosma, C., 2011. Optical dating of Romanian loess: A comparison between silt-sized and sand-sized quartz. Quat. Int. 240 (1–2), 62–70. https://doi.org/10.1016/j.quaint.2010.10.007.

Thiel, C., Buylaert, J.P., Murray, A.S., Terhorst, B., Hofer, I., Tsukamoto, S., Frechen, M., 2011. Luminescence dating of the Stratzing loess profile (Austria) - Testing the potential of an elevated temperature post-IR IRSL protocol. Quat. Int. 234 (1–2), 23–31. https://doi.org/10.1016/j.quaint.2010.05.018.

Ushko, K.A., 1959. Likhvin (Chekalin) section of interglacial deposits. In: Markov, K.K., Popov, A.I. (Eds.), Ice age in the European section of the USSR and in Siberia. Moscow State University Press, Moscow, pp. 148–226 (in Russian).

Vandenberghe, D., Corte, F.De., Buylaert, J.-P., Kučera, J., Van den haute, P., 2008. On the internal radioactivity in quartz. Radiation Measurements, 43(2-6), 771–775. https://doi.org/10.1016/j.radmeas.2008.01.016.

Van Vliet-Lanoë, B., 1998. Frost and soils: implications for paleosols, paleoclimates and stratigraphy. Catena 34 (1–2), 157–183. https://doi.org/10.1016/S0341-8162(98)00087-3.

Velichko, A.A., 1990. Loess-paleosol formation on the Russian Plain. Quat. Int. 7 (8), 103–114. https://doi.org/10.1016/1040-6182(90)90044-5.

Velichko, A.A. (Ed.), 2002. Dynamics of terrestrial landscape components and inner marine basins of Northern Eurasia during the last 130000 years. Atlas-monograph "Evolution of landscapes and climates of Northern Eurasia. Late Pleistocene – Holocene – elements of prognosis. II. General paleogeography". GEOS, Moscow. (in Russian).

Velichko, A.A., Morozova, T.D., 2015. Main features of soil formation within the Pleistocene on the East European Plain and their paleogeographical. In: Kudeyarov, V.N., Ivanov, I.V. (Eds.), Evolution of soil and soil cover. Theory, diversity of natural evolution and antropogenic transformations of soil. GEOS, Moscow, pp. 321–337 (in Russian).

Velichko, A.A., Morozova, T.D., Panin, P.G., 2007. Soil polygenetic complexes as a systematic phenomenon of Pleistocene macrocycles. Izv. Ross. Akad. Nauk. Ser. Geogr. 2, 44–54 (in Russian).

Velichko, A.A., Faustova, M.A., Pisareva, V.V., Gribchenko, Yu.N., Sudakova, N.G., Lavrentiev, N.V., 2011. Chapter 26 - Glaciations of the East European Plain: Distribution and Chronology. In: Ehlers, J., Gibbard, P.L., Hughes, P.D., (Eds.) Developments in Quaternary Sciences, 15, p. 337-359. doi: 10.1016/B978-0-444-53447-7.00026-X ISSN: 1571-0866, # 2011 Elsevier B.V.

Velichko, A.A., Morozova, T.D., Nechaev, V.P., Rutter, N.W., Dlusskii, K.G., Little, E.C., Catto, N.R., Semenov, V.V., Evans, M.E., 2006a. Loess/paleosol/cryogenic formation and structure near the northern limit of loess deposition, East European Plain. Russia. Quat. Int. 152–153, 14–30. https://doi.org/10.1016/j.quaint.2005.12.003.

Velichko, A.A., Semenov, V.V., Pospelova, G.A., Morozova, T.D., Nechaev, V.P., Gribchenko, Yu.N., Dlusskii, K.G., Rutter, N., Catto, N., Little, E., 2006b. Matuyama-Brunhes boundary in key sections of the loess–paleosol–glacial formations on the East European Plain. Quat. Int. 152–153, 94–102. https://doi.org/10.1016/j.quaint.2005.12.018.

Vepraskas, M.J., Lindbo, D.L., Stolt, M.H., 2018. Chapter 15 - Redoximorphic features. In: Stoops, G., Marcelino, V., Mees, F. (Eds.), Interpretation of Micromorphological Features of Soils and Regoliths (Second Edition). Elsevier, Amsterdam, pp. 425–445. https://doi.org/10.1016/B978-0-444-63522-8.00015-2.

Watanuki, T., Murray, A.S., Tsukamoto, S., 2005. Quartz and polymineral luminescence dating of Japanese loess over the last 0.6 Ma: Comparison with an independent chronology. Earth and Planetary Sci. Letters 240 (3–4), 774–789. https://doi.org/10.1016/j.epsl.2005.09.027.

Wintle, A.G., 1997. Luminescence dating: Laboratory procedures and protocols. Radiat. Meas. 27 (5–6), 769–817. https://doi.org/10.1016/S1350-4487(97)00220-5.

Wu, Y., Qiu, S., Fu, S., Rao, Z., Zhu, Z., 2018. Pleistocene climate change inferred from multi-proxy analyses of a loess-paleosol sequence in China. J. Asian Earth Sci. 154, 428–434. https://doi.org/10.1016/j.jseaes.2017.10.007.

Yakovleva, S.V., 1956. To the study of glacial boulders on the Russian Plain. Materials on Quaternary geology and geomorphology of the USSR. Moscow, New series 1, 18–43 (in Russian).

Zaidelman, F.R., 1974. Neubildungen hydromorpher mineralböden der UdSSR, IHRE klassifikation und diagnostische bedeutung. Geoderma 12 (1–2), 121–135. https://doi.org/10.1016/0016-7061(74)90044-5.

Zamanian, K., Pustovoytov, K., Kuzyakov, Y., 2016. Pedogenic carbonates: Forms and formation processes. Earth Sci. Rev. 157, 1–17. https://doi.org/10.1016/j.earscirev.2016.03.003.

Zeng, L., Lu, H., Yi, S., Stevens, T., Xu, Z., Zhuo, H., Yu, K., Zhang, H., 2017. Long-term Pleistocene aridification and possible linkage to high-latitude forcing: New evidence from grain size and magnetic susceptibility proxies from loess-paleosol record in northeastern China. Catena 154, 21–32. https://doi.org/10.1016/j.catena.2017.02.020.

Zykina, V.S., Zykin, V.S., Volvakh, A.O., Radaković, M.G., Gavrilov, M.B., Marković, S.B., 2020 (In Press). Late Pleistocene loess-paleosol sequence at the Belovo section, south of Western Siberia, Russia: Preliminary results. Quat. Int. https://doi.org/10.1016/j.quaint.2020.10.069.